

Effects of gravitational darkening on the determination of fundamental parameters in fast rotating B-type stars

Y. Frémat¹, J. Zorec², A.-M. Hubert³, and M. Floquet³

¹ Royal Observatory of Belgium, 3 avenue circulaire, B-1180 Bruxelles
e-mail: yves.fremat@oma.be

² Institut d'Astrophysique de Paris, CNRS, 98bis Boulevard Arago, F-75014 Paris

³ Observatoire de Paris, Section d'Astrophysique de Meudon, GEPI, FRE K 2459, 5 Place Jules Janssen, F-92195 Meudon CEDEX

Abstract. In this paper we develop a calculation code to account for the effects carried by fast rotation on the observed spectra of early-type stars. Stars are assumed to be in rigid rotation and the grid of plane-parallel model atmospheres used to represent the gravitational darkening are calculated by means of a non-LTE approach. Attention is paid on the relation between the *apparent* and *parent non-rotating counterpart* stellar fundamental parameters and apparent and true $V \sin i$ parameters as a function of the rotation rate Ω/Ω_c , stellar mass and inclination angle. It is shown that omission of gravitational darkening in the analysis of chemical abundances of CNO elements can produce systematic overestimation or underestimation, depending on the lines used, rotational rate and inclination angle. The proximity of Be stars to the critical rotation is re-discussed by correcting not only the $V \sin i$ of 130 Be stars, but also their effective temperature and gravity to account for stellar rotationally induced geometrical distortion and for the concomitant gravitational darkening effect. We concluded that the increase of the $V \sin i$ estimate is accompanied by an even higher value of the stellar equatorial critical velocity, so that the most probable average rate of angular velocity of Be stars attains $\Omega/\Omega_c \simeq 0.88$.

Key words. Stars: abundances – Stars: atmospheres – Stars: early-type – Stars: emission-line, Be – Stars: fundamental parameters – Stars: rotation

1. Introduction

Fast rotation produces a polar flattening and an equatorial stretching of stars, which in turn induce non-uniform surface gravity and temperature distributions: the gravity darkening effect (GD, Zeipel 1924). Owing to the levitation effect introduced by the rotation, rotating stars evolve as they had a lower mass: their core density is higher, the total bolometric luminosity produced is lower and they spend a longer time on the main sequence evolutionary phase than slowly rotating stars with the same mass (Sackmann 1970; Bodenheimer 1971; Clement 1979; Moss & Smith 1982; Meynet & Maeder 2000). The geometrical deformation of the star and the GD further influence the apparent status of the star, which also depends on whether it has a radiative or convective envelope (Lucy 1967; Tuominen 1972; Smith & Worley 1974; Claret 1998, 2000). As predicted by models of stellar evolution (Endal & Sofia 1979; Pinsonneault et al. 1991; Heger & Langer 2000; Meynet & Maeder 2000), fast rotation is further expected to generate several instabili-

ties that contribute to redistribute the internal angular momentum. They induce thus a turbulent diffusion in the stellar interior (Zahn 1992), which in massive objects drives the CNO-cycled material from the core to the envelope and changes the atmospheric chemical composition in these stars (Meynet & Maeder 2000).

1.1. Rotation dependent spectra of early type stars

Radiative and hydrostatic equilibrium conditions in atmospheres of rotating early-type stars impose in each point of the stellar surface the emitted bolometric flux be proportional to the local gravity $F \propto g_{\text{eff}}^\beta$ with $\beta \simeq 1$ if $T_{\text{eff}} \gtrsim 7000$ K and $g_{\text{eff}} = g_{\text{grav}} - g_{\text{rot}} + g_{\text{rad}}$ (Zeipel 1924; Claret 2000). Although a non-local theory of radiative transfer in rotating stars does not reproduce von Zeipel's relation, meridional circulation and turbulence in surface layers recover the validity of this law (Smith & Worley 1974). For B-type star effective temperatures, the radiation pressure g_{rad} can be neglected. Energy distributions, photometric indices and spectral lines produced in gravity-darkened early type rotating stars were calculated

by several authors, either for rigid (Collins 1963, 1965, 1966, 1968a,b, 1974; Hardorp & Strittmatter 1968b, 1972, 1968a; Hardorp & Scholz 1971; Collins & Sonneborn 1977; Collins et al. 1991; Maeder & Peytremann 1970, 1972) or for differential rotators with conservative internal rotational laws (Collins & Smith 1985; Zorec 1986). A0 to F5-type rigid rotators were studied by Pérez Hernández et al. (1999). The effects of the GD on the $V\sin i$ determinations were explored by Stoeckley (1968) for rigid rotators and Zorec et al. (1988) for differential rotators. Stoeckley (1968) concluded that the reduced contribution to the He I 4471 line broadening in the equatorial region may lead to underestimated rotational parameters in early-type stars, while Zorec et al. (1988a) obtained double valued $V\sin i$ in star models with polar hollows. Recently, Townsend et al. (2004) rediscussed the GD effect on the $V\sin i$ values of rigid early-type rotators and concluded that classic $V\sin i$ determinations for B0 to B9-type stars can be underestimated by 12 to 33% at $\omega = \Omega/\Omega_c = 0.95$ rotational rates, if the He I 4471 line is used and from 9 to 17%, if the Mg II 4481 line is studied.

1.2. Aim of the present work

Apart from the obvious rotation dependent Doppler effect, four factors, at least, still concur to produce the observed line broadening in gravity darkened fast rotators: a) changes with the surface non-uniform temperature of the continuous spectrum specific intensity; b) dependence of the intrinsic lines equivalent width with the local temperature and gravity; c) stretching of the isotherm and isogravity regions, which make that in strips of constant radial velocity for rather large Doppler displacements there can be temperatures close to that of the undistorted star; d) for high enough inclinations, the flattened stellar disc produce shortened constant Doppler displacement strips that tend to shallow the rotationally broadened line profile. A look on the He I 4471 and Mg II 4481 line equivalent width dependence with temperature and gravity can be obtained in Didelon (1982) and Sect. 4.3. These lines are currently used to determine the $V\sin i$ parameters of early-type stars (Slettebak et al. 1975). From classic model atmospheres we obtain that at the He I 4471 and Mg II 4481 line wavelengths the continuum specific intensity scales as $I_c \sim T_{\text{eff}}^a$, with $a \sim 2.2$ if $T_{\text{eff}} \gtrsim 7500$ K. Since is it $T_{\text{eff}}(\text{eq})/T_{\text{eff}}(\text{pole}) = (g_{\text{eq}}/g_{\text{pole}})^{0.25}$, we infer that for $\omega = 0.95$ the equatorial regions contribute less to the flux of the broadened line profile by a factor $I_c(\text{eq})/I_c(\text{pole}) \lesssim 0.2$ than in the pole. Line profiles are then expected to be narrower than those calculated with models where GD is neglected. At high aspect angles, effect d) compensates partially this deepening. Depending on the temperature of the star, in fast rotators the change of the local T_{eff} and $\log g$ with latitude produce the equivalent width of the He I 4471 line be either $W_{\text{HeI}}(\text{eq}) > W_{\text{HeI}}(\text{pole})$, or $W_{\text{HeI}}(\text{eq}) < W_{\text{HeI}}(\text{pole})$, while the equivalent width of the Mg II 4481 line is always

$W_{\text{MgII}}(\text{eq}) > W_{\text{MgII}}(\text{pole})$. Let us note that for the He I 4471 line, we actually mean the blend He I 4471+He I 4470, where the second line is a forbidden component and has a somewhat different sensitivity to fundamental parameters than the permitted $\lambda 4471$ component. For the He I 4471 and Mg II 4481 lines also respond in a different way to the GD and because they overlap partially, the $V\sin i$ determination demands that we proceed to fit both lines simultaneously.

The aim of this paper is thus to take into account, as properly as possible, the changes of the stellar radii R_{pole} and R_{eq} and of the global bolometric luminosity with ω in the calculation of the emitted radiation fluxes. We will also fit both He I 4471 and Mg II 4481 lines in order to determine up to what degree the $V\sin i$ parameters of early-type fast rotators are underestimated if they are obtained assuming that rotational distortion and GD can be neglected. This is of particular interest for Be stars to know whether they are near-critical rotators (Townsend et al. 2004). In this paper, we will also discuss the effect of the rapid rigid rotation on the determination of the stellar effective temperature, surface gravity and chemical composition.

2. Model atmospheres

Fast rotation flattens the star and produces non-uniform density and temperature distributions in its surface. To take into account the first order effects of this flattening on the stellar spectrum of B-type stars, we adopted a method similar to the one described by Collins et al. (1991), but modified to introduce the changes detailed in Sect. 2.1. In this approach, that we applied in a computer code hereafter named FASTROT, the stellar photosphere is replaced by a mesh of plane-parallel model atmospheres depending each on the local temperature and surface gravity (Sect. 2.2).

2.1. Flattening and gravitational darkening

We assume that the stars are rigid rotators without any surface latitudinal differential rotation component. We adopted the Roche approximation for the stellar surface equipotentials, i.e. in the gravity potential the dipole and higher order terms are neglected (Tassoul 1978). In the expression of the surface effective gravity we also neglected the latitude-dependent radiation pressure term ($g_{\text{rad}} = 0$; Maeder & Meynet 2000). From the Roche equipotentials it follows that the ratio between the equatorial to the polar radii at the rotational rate $\omega = \Omega/\Omega_c$ ($\Omega_c =$ critical angular velocity) is given by:

$$\left. \begin{aligned} \frac{R_e(\omega)}{R_p(\omega)} &= 1 + \frac{1}{2}\eta \\ \eta &= \omega^2 \left(\frac{R_e(\omega)}{R_c} \right)^3 \end{aligned} \right\} \quad (1)$$

where R_c is the equatorial radius at critical rotation ($\omega = 1$).

In what follows we use the Ω/Ω_c to characterize the rotation rate instead of V_e/V_c where V_e and V_c are the actual and critical linear equatorial rotation velocities respectively. The main reason for this choice is that as we assume stars are rigid rotators, the angular velocity Ω , which is the same over the whole star (surface and interior) and independent of any other stellar quantity, it can be considered as an independent fundamental parameter. We note, however, that the stellar rotational distortion and the associated gravity darkening effect are controlled by the parameter η given in (1). Though Ω/Ω_c , V_e/V_c and η are functions having the same germs 0 and 1, it is $\Omega/\Omega_c < V_e/V_c < \eta$ in the open interval $0 < \Omega/\Omega_c < 1$.

In previous works it is often assumed that $R_p(\omega) = R_o$ where R_o is the radius of the star at rest (Collins et al. 1991; Reiners 2003; Townsend et al. 2004). In the present study we adopted instead the following interpolation expression for R_p , derived from the calculations performed by Bodenheimer (1971), Clement (1979) and Zorec et al. (1988):

$$\left. \begin{aligned} \frac{R_p(\omega)}{R_o} &= 1 - P(M)\tau \\ P(M) &= 5.66 + \frac{9.43}{M^2}, \quad \text{for } M \gtrsim 2 \end{aligned} \right\} \quad (2)$$

where M is the stellar mass in solar units and $\tau = K/|W|$ with K the rotational kinetic energy and W the stellar gravitational potential energy. A rough relation between τ and η is given by $\tau \simeq [0.0072 + 0.008\eta^{1/2}]\eta^{1/2}$. Although (1) implies $R_c = 1.5R_o$ at critical rotation, as from (2) $R_p(\omega) < R_o$, depending on the B-type stellar mass, it is $R_c = 1.3R_o$ to $1.4R_o$, rather than $R_c = 1.5R_o$ as usually assumed in the literature.

The total bolometric luminosity produced in the stellar core was assumed given by:

$$L(\omega, M, g_o) = L_o(M, g_o)f_L(\tau, M) \quad (3)$$

where L_o is the bolometric luminosity of an homologous non-rotating star with mass M and rest surface gravity g_o . The expression for the factor f_L was derived from Clement's (1979) models for $M \gtrsim 1.5$:

$$\left. \begin{aligned} f_L &= a(M) + [1 - a(M)]e^{-b(M)\tau} \\ a(M) &= 0.675 + 0.046M^{1/2} \\ b(M) &= 52.71 + 20.63M^{1/2} \end{aligned} \right\} \quad (4)$$

The quoted models (Bodenheimer 1971, Clement 1979, Zorec et al. 1988b) were calculated for stars with internal conservative differential rotation laws and for energy ratios τ that reach the global secular stability limit $\tau = K/|W| \simeq 0.14$ and even higher. In all these models the core is supposed to rotate as a rigid body. Moreover, these calculations show that the radii ratio $R_p(\omega)/R_c$ and the function f_L do not depend on the rotation law in the stellar envelope (Zorec 1986). Nevertheless, the interpolation relations (2) and (4) are for $0 \leq \tau = K/|W| \lesssim 0.03$, range of τ values which are suited for rigid rotators, including the rigid critical rotation, where $\tau = K/|W| \lesssim 0.02$ whatever the stellar mass in the $2 \lesssim M \lesssim 60$ range.

Relation (3) takes into account only the change of the total bolometric luminosity due to the mechanic rotationally induced changes of the stellar core temperature and pressure (Sackmann 1970). Whenever possible, we have checked that the changes introduced by mixing phenomena induced by the instabilities produced by the rotation (Endal & Sofia 1976; Maeder & Meynet 1996; Meynet & Maeder 2000) do not introduce significant changes to the f_L given by 4.

In this work the GD law was written as:

$$T_{\text{eff}}^4(\theta, \omega) = \gamma(\omega, M, R_o)g^\beta(\theta, \omega) \quad (5)$$

where θ is the colatitude angle; M is the stellar mass; R_o is the radius of the star at rest; g is the modulus of the gravity vector $\vec{g} = -\nabla\Phi$ with Φ being the Roche potential; β was considered = 1 for all local $T_{\text{eff}}(\theta, \omega) \gtrsim 7000$ K. For lower local T_{eff} , β was interpolated in Claret (1998). The factor γ was calculated for each ω as follows:

$$\gamma = \frac{L(\omega, M, g_o)}{\sigma \int_{\mathcal{S}} g^\beta d\mathcal{S}} \quad (6)$$

where σ is the Štefan-Boltzmann constant and \mathcal{S} is the total area of the surface Roche equipotential. From (3) it comes that the global effective temperature $\overline{T_{\text{eff}}} = [L(\omega)/\sigma\mathcal{S}]^{1/4}$ is smaller than $T_{\text{eff}}^\circ = [L_o/4\pi\sigma R_o^2]^{1/4}$, the effective temperature of a non-rotating star with the same mass. On the other hand, relations (5) and (6) imply that $T_{\text{eff}}(\omega)_{\text{pole}} > \overline{T_{\text{eff}}}$. In the literature relation (5) is currently replaced by $T_{\text{eff}}^4(\theta, \omega) = T_{\text{eff}}^4(\theta=0, \omega)[g(\theta, \omega)/g(\theta=0, \omega)]^\beta$, which hinders to relate the apparent stellar fundamental parameters with those the star would had if it were at rest. We note that the relations $T_{\text{eff}}(\theta=0, \omega) = T_{\text{eff}}^\circ$ and $g(\theta=0, \omega) = g_o$, where T_{eff}° and g_o are the fundamental parameters of the rotationless star, do not hold and that only the effective temperature and gravity averaged over the whole polar-on seen stellar hemisphere approach the effective temperature T_{eff}° and gravity g_o roughly, i.e.: $\lim_{i \rightarrow 0} \langle T_{\text{eff}}(\theta, \omega|i) \rangle \sim T_{\text{eff}}^\circ$ and $\lim_{i \rightarrow 0} \langle g(\theta, \omega|i) \rangle \sim g_o$. In all cases it is $T_{\text{eff}}(\theta=0, \omega) \geq T_{\text{eff}}^\circ$ and $g(\theta=0, \omega) \geq g_o$.

2.2. Local plane-parallel models

The spectrum of a rotating star is represented as the intensity of radiation emitted per unit wavelength interval per steradian in the direction towards the observer defined by the aspect angle i (inclination angle of the stellar rotation axis with respect to the line of sight). It is given by (Collins 1965; Maeder & Peytremann 1970):

$$L_\lambda(i, \omega) = 2 \int_0^{\pi/2} d\phi \int_0^\pi R^2(\theta) I_\lambda(\mu, \omega) \frac{|\mu|}{\cos \delta} \sin \theta d\theta \quad (7)$$

where $R(\theta)$ is the co-latitude θ -dependent distance between the stellar center and the surface of the rotation ally-distorted star; $\mu = \mu(\phi, \omega) = \hat{n} \cdot \hat{i}$ (\hat{n} is the unit vector normal to the stellar surface and \hat{i} is the unit vector representing the direction of the line of sight);

$\cos \delta(\theta, \omega) = -\hat{n} \cdot \hat{r}$ (\hat{r} is the unit vector in the direction of $R(\theta)$); $I_\lambda(\mu, \omega)$ is the μ -dependent monochromatic specific radiation intensity calculated for the local effective temperatures $T_{\text{eff}}(\theta, \omega)$ and surface gravities $g(\theta, \omega)$. The integration of equation (7) was performed using a Gauss-biquadrature of degree 96 in both angles θ and ϕ , which in principle is equivalent to a grid of 36481 surface elements of local plane-parallel model atmospheres. Each stellar surface point was characterized by its specific radial velocity in the observer's direction in order to take into account the corresponding Doppler shift in the spectral line.

The models we used to evaluate each local specific intensity $I_\lambda(\mu, \omega)$ were computed in two consecutive steps. To account in the most effective way for the line-blanketing, the temperature structure of the atmospheres have been computed as in Kurucz & Castelli (2000) using the ATLAS9 computer code (Kurucz 1993). Non-LTE level populations were then computed for each of the atoms we considered using TLUSTY (Hubeny & Lanz 1995) and keeping fixed the temperature and density distributions obtained with ATLAS9.

Excepted for C II, the atomic models we used in this work were downloaded from TLUSTY's homepage (<http://tlusty.gsfc.nasa.gov>) maintained by I. Hubeny and T. Lanz. Table 1 lists the ions that were introduced in our computations. C II was treated with use of the MODION IDL package developed by Varosi et al. (1995) and by adopting the atomic data (oscillator strengths, energy levels and photoionization cross-sections) selected from the TOPBASE database (Cunto et al. 1993). It reproduces the results obtained by Sigut (1996).

In this way and for each spectral region studied in the present work, the specific intensity grids were computed for effective temperatures and surface gravities ranging respectively from 15000 K to 27000 K and from 3.0 to 4.5. For $T_{\text{eff}}^o < 15000$ K and $T_{\text{eff}}^o > 27000$ K (T_{eff}^o concern rotationless model atmospheres) we used LTE calculations and the OSTAR2002 model atmospheres grid (Lanz & Hubeny 2003).

3. Comparison of rotating with non-rotating models

3.1. Adopted procedure

Hydrogen and helium line profiles, more particularly, the $H\gamma$, $\lambda 4388$ He I and $\lambda 4471$ He I lines, are often used to derive the effective temperature, surface gravity and projected rotation velocity of B type stars. Among the reasons of their use, we have: 1) the line profiles and equivalent widths are very sensitive to effective temperature and surface gravity; 2) the blue helium lines are known to be somewhat less sensitive to LTE departures; 3) the broadening mechanisms of their line profiles have been well known for a long time (e.g.: Barnard et al. 1969; Leckrone 1971; Vidal et al. 1973; Mihalas et al. 1974).

Table 1. Atomic models used

Atom	Ion	Description
Hydrogen	H I	8 levels + 1 superlevel
	H II	1 level
Helium	He I	24 levels
	He II	20 levels
	He III	1 level
Carbon	C II	53 levels all individual levels
	C III	12 levels
	C IV	9 levels + 4 superlevels
	C V	1 level
Nitrogen	N I	13 levels
	N II	35 levels + 14 superlevels
	N III	11 levels
	N IV	1 level
Oxygen	O I	14 levels + 8 superlevels
	O II	36 levels + 12 superlevels
	O III	9 levels
	O IV	1 level
Magnesium	Mg II	21 levels + 4 superlevels
	Mg III	1 level

Table 2. Sets of parameters used in model grids

GRIDA				
5000 K	\leq	T_{eff}^o	\leq 40000 K	step = 1000 K
2.5	\leq	$\log g_o$	\leq 5.0	step = 0.5
0 km s ⁻¹	\leq	$V \sin i$	\leq 500 km s ⁻¹	step = 50 km s ⁻¹
GRIDB				
12000 K	\leq	T_{eff}^o	\leq 27000 K	step = 1000 K
3.2	\leq	$\log g_o$	\leq 4.4	step = 0.2
0°	\leq	i	\leq 90°	step = 5°
0.50	\leq	Ω/Ω_c	\leq 0.99	step = 0.05

Two grids of spectra ranging from 4250 Å to 4500 Å were computed. A first grid, GRIDA, was obtained using classical plane-parallel model atmospheres. A second grid, GRIDB, was calculated using FASTROT (Sect. 2) where stellar flattening and gravity darkening are taken into account. The sets of fundamental parameters considered in these grids are given in Table 2. T_{eff}^o and g_o refer to the fundamental parameters of the rotationless or parent non-rotating counterpart of the star (Sect. 2.1). Regarding the notation, it is worth noting that for GRIDA it holds $T_{\text{eff}} = T_{\text{eff}}^o$ and $\log g = \log g_o$.

In what follows we will determine the effective temperature, surface gravity and the projected rotational velocity of B-type stars using only the $H\gamma$, He I 4388, He I 4471 and Mg II 4481 lines. To this end we will use a fitting procedure based on a least-squares method that applies the MINUIT minimization package available at CERN. In order to know the confidence degree of this method, we fitted the spectra of the GRIDA reference library using synthetic spectra obtained from the same NLTE plane-parallel model atmospheres like the GRIDA spectra. The free, or fit parameters used to this purpose were: the ef-

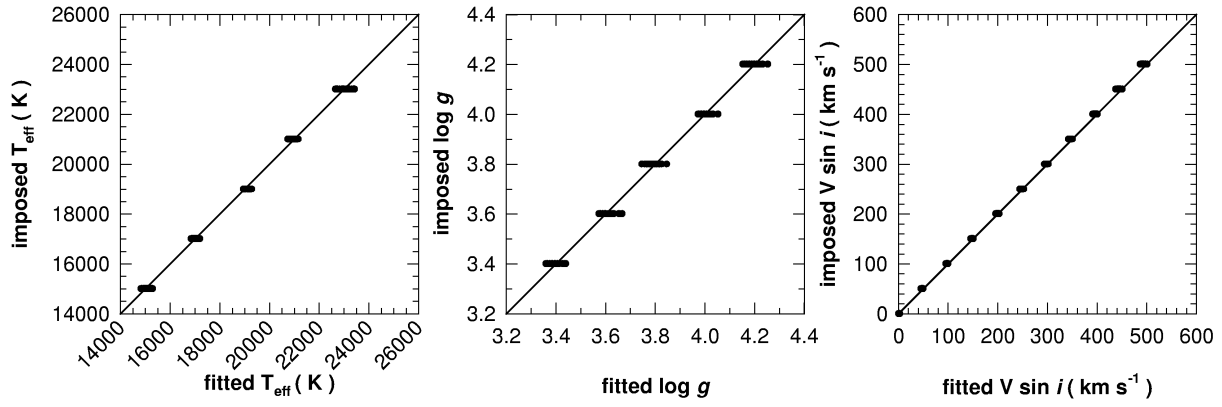


Fig. 1. Test of the adopted procedure: comparison of T_{eff} , $\log g$ and $V \sin i$ parameters obtained by the fitting procedure with the model parameters of GRIDA

Table 3. Spectral regions considered for the fits.

Spectral line	CASE		$\Delta \lambda$ (Å)
	A	B	
H γ	×	×	4300 - 4375
$\lambda 4388$ He I	×	×	4375 - 4400
$\lambda 4471$ He I		×	4460 - 4475
$\lambda 4471$ He I + $\lambda 4481$ Mg II	×		4460 - 4490

fective temperature, surface gravity, the projected rotational velocity and the averaged flux ratio of the fitted to the reference spectrum. The χ^2 deviation parameter was computed only for the selected spectral domains defined in Table 3 for CASE A. The comparison shown in Fig. 1 of parameters obtained by the minimization procedure with the model GRIDA reference parameters, reveals that the agreement is quite satisfactory. However, this agreement is the best for the projected rotational velocity, whose accuracy is generally better than 4%. The derived effective temperature approaches the most to the reference values when $T_{\text{eff}} \sim 20000$ K, but for other temperatures deviations never exceed 500 K. The errors committed on $\log g$ are always lower than 0.05 dex whatever the effective temperature.

To study the effects of fast rotation on the determination of stellar fundamental parameters, we applied the same procedure than above to the GRIDB spectra, where the model parameters are $\{T_{\text{eff}}^{\circ}, \log g_{\circ}, i, \Omega/\Omega_c\}$ or equivalently $\{T_{\text{eff}}^{\circ}, \log g_{\circ}, V \sin i, \Omega/\Omega_c\}$. Since the fit of spectra produced by rotating stars can be done in two ways, we distinguish two sets of parameters. The reference model parameters proper to calculate FASTROT rotationally modified synthetic spectra, as well as those obtained by fitting with them the rotationally distorted spectra, are hereafter called *parent non-rotating counterpart (pnrc)* fundamental parameters and will be noted with a superscript “ \circ ” or a subscript “ \circ ” (i.e. T_{eff}° and $\log g_{\circ}$), while $V \sin i$ will represent the true projected rotation velocity of the star. Conversely, we call *apparent* fundamental parameters (i.e. $T_{\text{eff}}^{\text{app}}$, $\log g_{\text{app}}$ and $V \sin i_{\text{app}}$), those derived by fitting the

GRIDB spectral lines with synthetic spectra issued from classical plane-parallel model atmospheres.

The fit of the H γ , He I 4388 and He I 4471 lines was done either including the Mg II 4481 line or excluding it in order to test the procedure’s sensitivity to a change of the fitting criteria; this identifies respectively CASE A or CASE B in Table 3.

3.2. Reference parameters

In the following sections, calculations will be done for several effective temperatures and surface gravities. To have a rough look on the spectral types they may concern as well as the relations that exist between the fundamental parameters suited for non-rotating stars and the apparent ones – which are dependent on the stellar geometrical distortions and the concomitant GD – we list in Table 4 the reference parameters we used in the present work. In this table are also given the polar effective temperature and the polar radius of the distorted stars for several values of the angular velocity ratio Ω/Ω_c .

The MK spectral types adopted (Gray & Corbally 1994) are for the effective temperatures and $\log g_{\circ} = 4.0$ of the *parent* non-rotating stars. The stellar masses and radii for $\Omega/\Omega_c = 0$ used to calculate the critical velocity V_c (c.f Sect. 2.1) were derived from stellar evolutionary tracks of non-rotating stars (Schaller et al. 1992).

4. Apparent fundamental parameters

Following the procedure described in Section 3.1, we obtained a grid of *pnrc* (i.e.: parameters belonging to the parent non-rotating stellar counterpart) and *apparent* fundamental parameters for different values of the angular velocity and inclination angle of the star. Since the aim of the present computations is to provide a way to correct the observed fundamental parameters from gravitational darkening effects for a large parameter-space, in the present work we have chosen to present the effects due to fast rotation and the corresponding corrections, as a function of $T_{\text{eff}}^{\text{app}}$, $\log g_{\text{app}}$ and $V \sin i_{\text{app}}$ (e.g. Fig. 2),

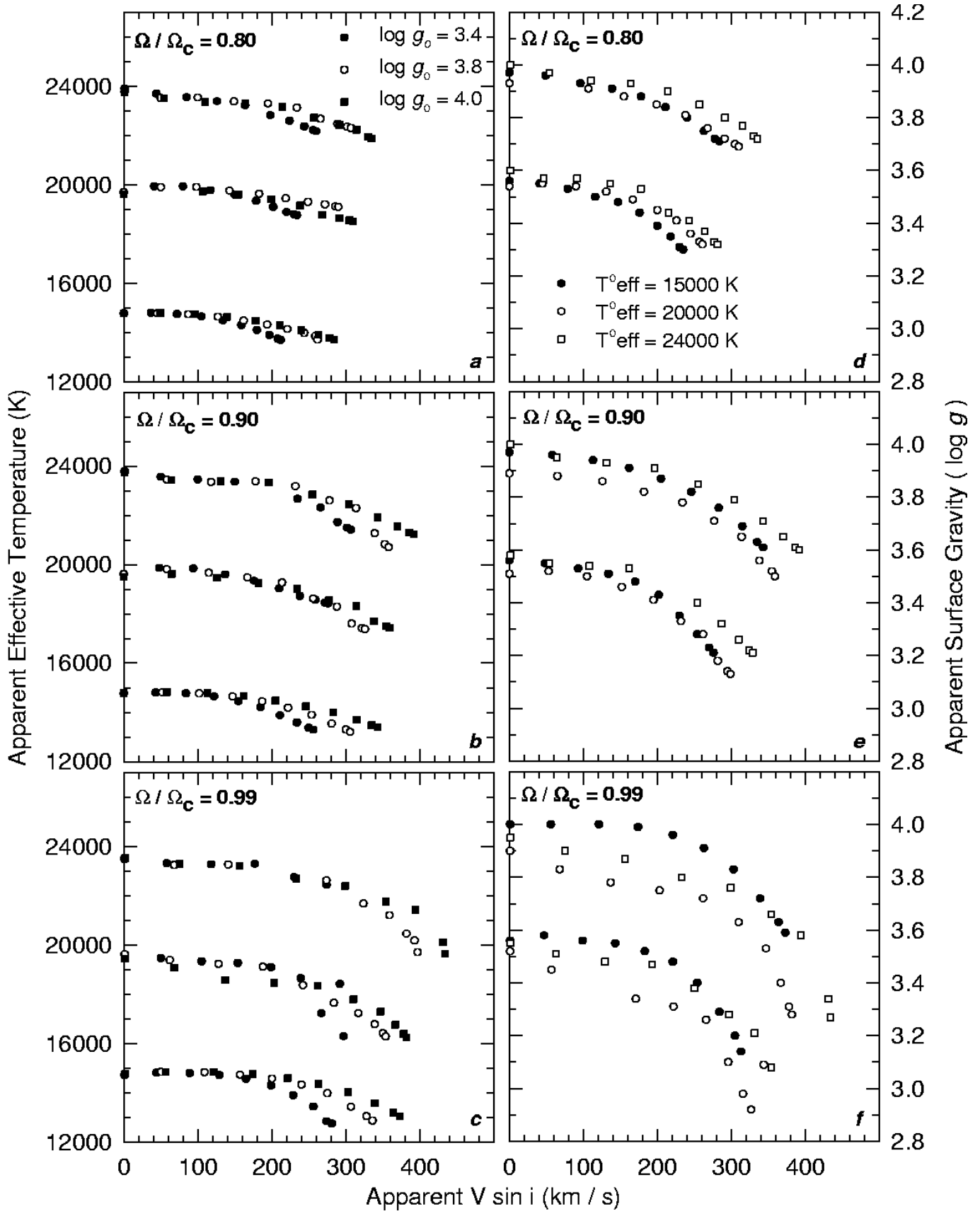


Fig. 2. Apparent effective temperature and surface gravity as a function of $V \sin i$ for different pnrc ($T_{\text{eff}}^o, \log g_o$) values and rotation rates Ω / Ω_c

Table 4. Polar temperature (T_{polar}), polar radii (R_{p}) and critical velocities (V_{c}) as a function of Ω/Ω_{c} and for $\log g_{\text{o}} = 4$.

MK Type	$T_{\text{eff}}^{\text{o}}$ K	Mass M_{\odot}	Ω/Ω_{c}	T_{polar} K	R_{p} R_{\odot}	V_{c} km/s
B1 V	24620	10.53	0.00	24620	5.32	525
			0.50	24932	5.22	
			0.80	25887	5.10	
			0.99	27593	4.88	
B2 V	19500	6.87	0.00	19500	4.30	472
			0.50	19736	4.21	
			0.80	20471	4.11	
			0.99	21773	3.94	
B5 V	14000	4.15	0.00	14000	3.34	418
			0.50	14176	3.27	
			0.80	14708	3.19	
			0.99	15609	3.04	
B9 V	10720	2.86	0.00	10720	2.77	383
			0.50	10870	2.71	
			0.80	11300	2.63	
			0.99	12007	2.50	

Table 5. Effects of fast rotation in equator-on B type stars. The effective temperature (RT_{eff}) and surface gravity ($R\log g$) underestimation percentage are given against Ω/Ω_{c} .

Ω/Ω_{c}	RT_{eff}	$R\log g$
0.80	9 %	8 %
0.90	12 %	10 %
0.99	17 %	20 %

to make a direct link with the actually measured quantities, rather than against the pnrc fundamental parameters, which need to be determined from the sought corrections. As the REFs are strongly dependent on the aspect angle i , we present them as a function of the observed $V\sin i_{\text{app}}$.

4.1. Effective temperature

The typical effects of stellar flattening and GD on effective temperature are shown in Fig. 2 for different combinations of $T_{\text{eff}}^{\text{o}}$ and $\log g_{\text{o}}$, while the corrections ΔT_{eff} to add to the *apparent* effective temperature to get the pnrc effective temperature at different apparent Ω/Ω_{c} , apparent $V\sin i$, and apparent $\log g$ regimes are plotted in Fig. 3 (upper panel). As expected, the $T_{\text{eff}}^{\text{app}}$ decreases with increasing $V\sin i_{\text{app}}$. Fast rotation produces therefore a lowering of the apparent effective temperature. Concerning the amplitude of this effect and its general behaviour, the following remarks can be made:

- i*) REFs on $T_{\text{eff}}^{\text{app}}$ become significant for $\Omega/\Omega_{\text{c}} > 0.6$. They are stronger and vary more rapidly with $V\sin i_{\text{app}}$ the larger the values of Ω .

- ii*) When Ω/Ω_{c} increases, REFs on $T_{\text{eff}}^{\text{app}}$ become more sensitive to surface gravity in the sense that they are larger the lower is the gravity.
- iii*) The relative lowering effect on the apparent T_{eff} does not depend much on its pnrc value. In Table 5 this effect is given in percentages for different angular velocities in stars seen equator-on, where effects are the stronger.
- iv*) When studying dwarf B-type stars, REFs on $T_{\text{eff}}^{\text{app}}$ can be ignored safely at $V\sin i_{\text{app}}$ lower than 200 km s^{-1} and at $V\sin i_{\text{app}} \lesssim 100 \text{ km s}^{-1}$ for giant B-type stars.

4.2. Surface gravity

Corrections $\Delta\log g$ to add to the *apparent* surface gravity to get the pnrc surface gravity at different Ω/Ω_{c} , apparent $V\sin i$ and apparent T_{eff} regimes are plotted in Fig. 3 (lower panel). As shown in Fig. 2, stellar flattening and gravitational darkening produce a lowering of the apparent surface gravity. The amplitude of this REF varies obeying the following rules:

- i*) REFs on $\log g_{\text{app}}$ become significant for $\Omega/\Omega_{\text{c}} > 0.6$. They are stronger and vary more rapidly with $V\sin i_{\text{app}}$ at high Ω/Ω_{c} values.
- ii*) When $\Omega/\Omega_{\text{c}} \lesssim 0.85$, REFs on $\log g_{\text{app}}$ are weaker in stars with $T_{\text{eff}}^{\text{o}} \gtrsim 20000 \text{ K}$ than in those with $T_{\text{eff}}^{\text{o}} \lesssim 20000 \text{ K}$. On the contrary, for $\Omega/\Omega_{\text{c}} \gtrsim 0.85$, the apparent $\log g$ are more sensitive to REFs in stars with $T_{\text{eff}}^{\text{o}} \gtrsim 20000 \text{ K}$ than in those with $T_{\text{eff}}^{\text{o}} \lesssim 20000 \text{ K}$. This change in the $\log g$ sensitivity to REFs, according to $T_{\text{eff}}^{\text{o}}$ and Ω/Ω_{c} , is due to hydrogen lines, which in the present approach are the main $\log g$ indicators. In hot stars, the intensity of hydrogen lines is the lowest, but it increases fast with the equatorial local T_{eff} decrease produced by increasing values of Ω/Ω_{c} .
- iii*) The lowering of $\log g_{\text{app}}$ does not depend much on the pnrc $\log g$ value. It is given in percentages in Table 5 for different angular velocities in stars seen equator-on where effects are the stronger. In the more distorted cases, the change in $\log g_{\text{app}}$ represents two luminosity classes.
- iv*) In B-type stars with $T_{\text{eff}}^{\text{app}} \lesssim 18000 \text{ K}$ and $V\sin i_{\text{app}} \lesssim 100 \text{ km s}^{-1}$, REFs on $\log g$ can be ignored.

4.3. Projected rotation velocity

The REFs on $V\sin i_{\text{app}}$ become significant for $\Omega/\Omega_{\text{c}} \gtrsim 0.70$. The spectral lines become progressively less broadened than expected from models of stars without GD, due to a lower contribution to the line flux coming from the gravity darkened equatorial regions towards the stellar limb. The magnitude of this effect depends on the sensitivity of the line studied to the local changes of T_{eff} and $\log g$, as shown in Fig. 4 for the He I 4471 and for the Mg II 4481 lines.

At a given $\Omega/\Omega_{\text{c}} \gtrsim 0.7$ and $T_{\text{eff}}^{\text{o}} \lesssim 18000 \text{ K}$, the broadening of the He I 4471 line tends to saturate for

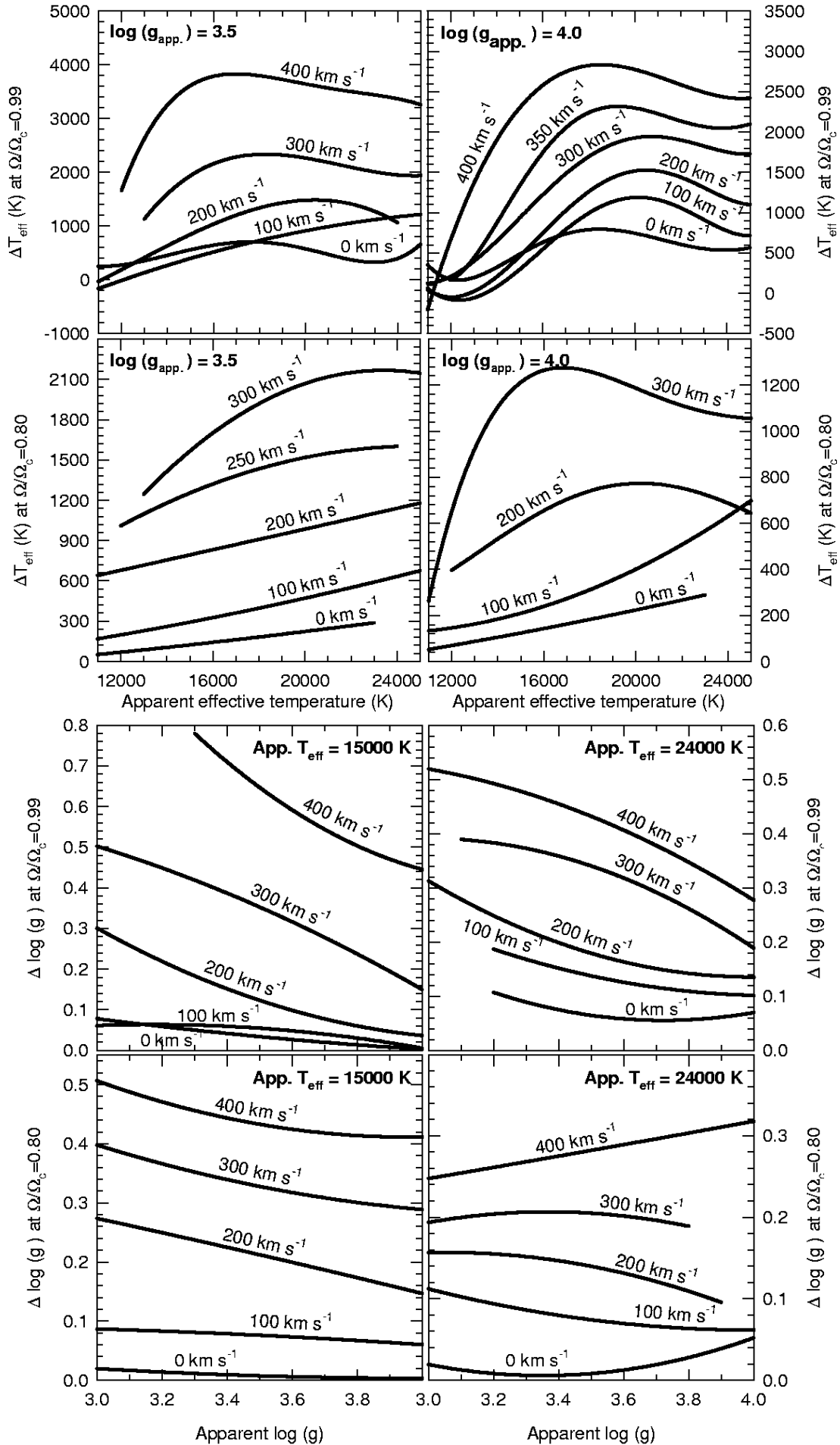


Fig. 3. Upper panel: Corrections ΔT_{eff} to add to the apparent effective temperature ($T_{\text{eff}}^{\text{app}}$) for different Ω/Ω_c , $V \sin i_{\text{app}}$, and $\log g_{\text{app}}$. Lower panel: Corrections $\Delta \log g$ to add to the apparent surface gravity for different Ω/Ω_c ,

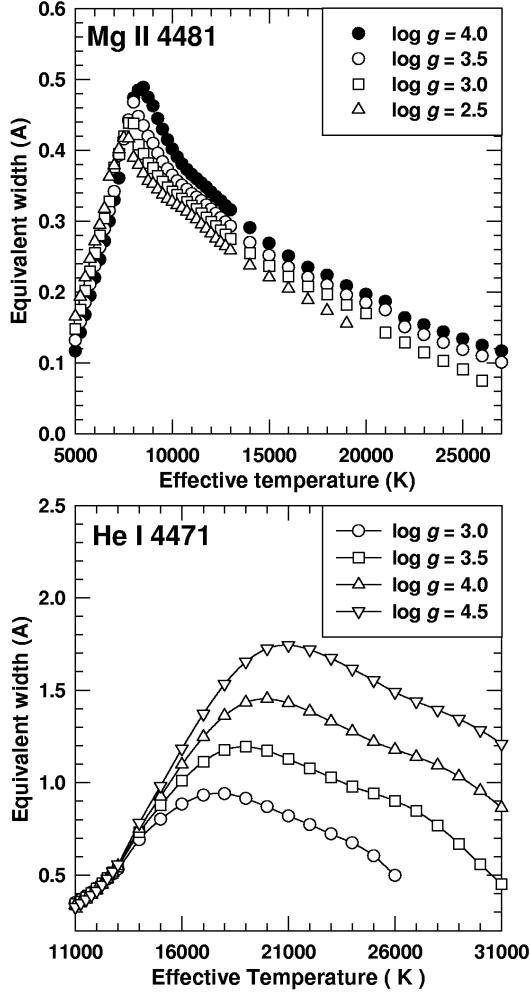


Fig. 4. Equivalent widths of the He I 4481 and Mg II 4481 spectral lines against effective temperature for different $\log g$ values. Computations were made assuming plane-parallel model atmospheres.

increasing values of $V \sin i_{\text{app}}$. In stars cooler than $T_{\text{eff}}^{\circ} \simeq 18000$ K, the saturation of this broadening is favored also by the enhanced contribution to the line flux from the polar regions, where the local T_{eff} is increased by the GD. Fig. 5 shows the apparent $V \sin i_{\text{FFT}}$ against true $V \sin i$ for $\log g_{\circ} = 4.0$, $\Omega/\Omega_{\text{c}} = 0.99$ and for different values of T_{eff}° when only the He I 4471 line (Fig. 5 a) is considered. The apparent $V \sin i$ parameter is obtained in this figure using the Fourier transform method applied to line profiles calculated with FASTROT. In the present work, the Fourier method is meant to represent the classical techniques of determining rotational parameters. We see that in a star having a $T_{\text{eff}}^{\circ} = 14000$ K, a $V \sin i_{\text{app}} \simeq 250$ km s $^{-1}$ value implies that the underestimation of the projected rotational velocity is $\delta V \sin i = (V \sin i) - (V \sin i_{\text{app}}) \simeq 140$ km s $^{-1}$, if it rotates at $\Omega/\Omega_{\text{c}} = 0.99$. The underestimation $\delta V \sin i$ drops fast as soon as $\Omega/\Omega_{\text{c}} < 0.99$, while the magnitude of the $V \sin i_{\text{app}}$ saturation depends on the inclination angle, angular velocity and also on the effective temperature (e.g. Fig. 5, 6, 8 and 7).

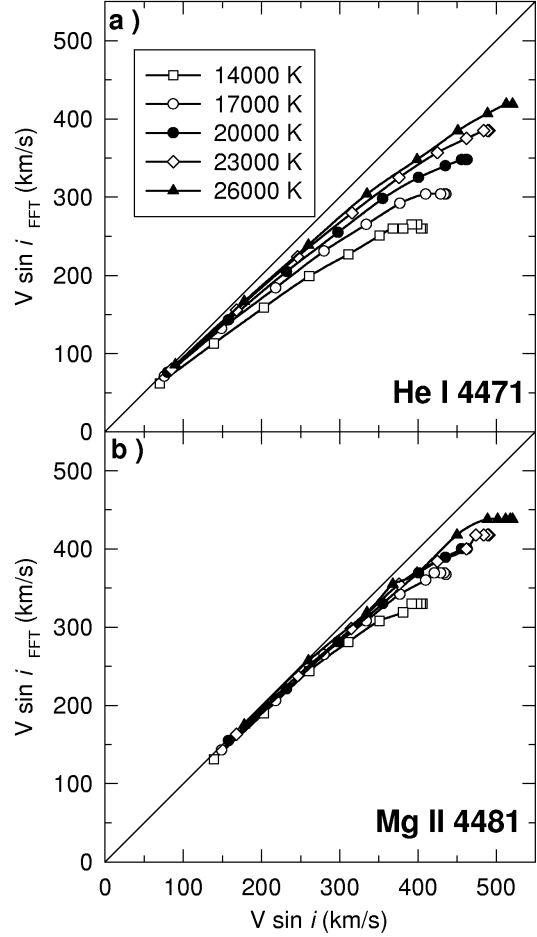


Fig. 5. Apparent $V \sin i$ derived using the Fourier Transform technique against the true $V \sin i$ considering individually the He I 4471 line (panel a) and Mg II 4481 spectral line (panel b). Computations are made assuming $\Omega/\Omega_{\text{c}} = 0.99$.

Same conclusions can be drawn for the Mg II 4481 line. However, in this case the above mentioned line broadening underestimation is less pronounced (Fig. 5 b). This is due to the fact that the intensity of the Mg II 4481 line is smaller in the polar regions than in the equatorial, so that even the continuum intensity in the line wavelengths is stronger at the pole than in the equator. The differentiated response of the continuum and the intrinsic line intensity to T_{eff} and $\log g$ compensate to each other somewhat, producing hence a smaller $\delta V \sin i$.

The relation between the apparent and the true $V \sin i$ derived from the Mg II 4481 is shown in Fig. 5. We note in this figure that saturation effects are seen in the He I 4471 line for low T_{eff}° values and in the Mg II 4481 line when T_{eff}° is high. In the first case, the effect is due to a significant decrease of the equivalent width of the line for low effective temperatures (i.e. at the stellar equator). In the second case, the contrast of the continuum specific intensity between the pole and the equator cannot be compensated by the modest increase of the equivalent width of the line at lower equatorial temperatures (cf. Fig. 4).

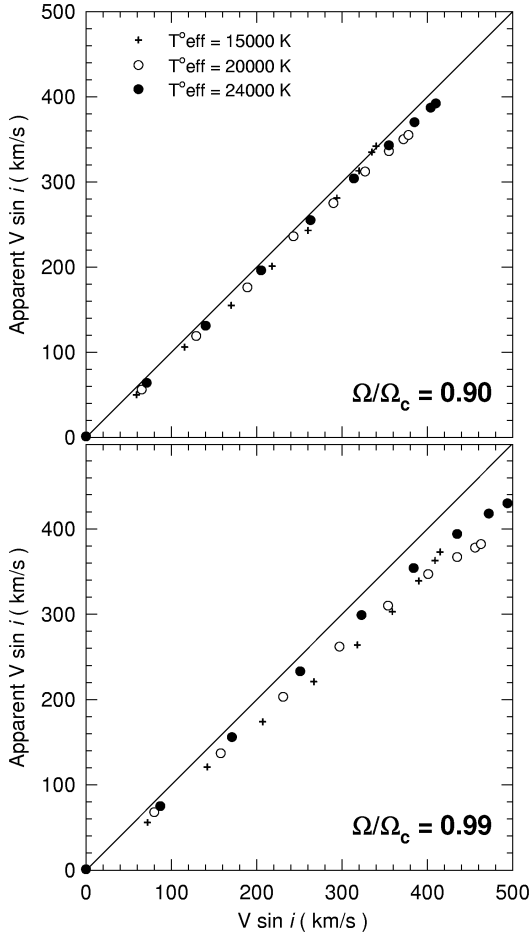


Fig. 6. Comparison between true and apparent $V \sin i$ in fast rotating stars assuming $\log g_{\text{app}} = 4$. The fitted regions correspond to CASE A of Table 3.

As can be seen in Fig. 6, where $V \sin i_{\text{app}}$ was derived following the procedure described in Sect. 3.1, the simultaneous fitting of various spectral lines combined with the simultaneous determination of $T_{\text{eff}}^{\text{app}}$, $\log g_{\text{app}}$ and $V \sin i_{\text{app}}$ limits somewhat the saturation effect and minimizes the underestimation of the projected rotation velocity at high inclinations and angular velocity rates. Fig. 6 shows the relation between the apparent and true $V \sin i$ for $\Omega/\Omega_c = 0.80$, $\Omega/\Omega_c = 0.99$, $\log g_o = 4.0$ and for different T_{eff}^o values when both He I 4471 and Mg II 4481 lines are taken into account for the $V \sin i$ determination. Considering the case $\Omega/\Omega_c = 0.99$ (i.e. $V_e/V_c \simeq 0.97$), we see that for whatever pnc T_{eff}^o , the apparent $V \sin i$ underestimates the true rotation by $\delta V \sin i \lesssim 50 \text{ km s}^{-1}$ as far as the apparent $V \sin i \lesssim 350 \text{ km s}^{-1}$. Underestimations may then increase to $\delta V \sin i \simeq 80 \text{ km s}^{-1}$ for apparent $V \sin i \gtrsim 350 \text{ km s}^{-1}$. It is worth noting the peculiar behavior of this relation for the $T_{\text{eff}}^o = 15000 \text{ K}$. The enhanced contribution of the Mg II 4481 line to the blend He I 4471+Mg II 4481 at high inclinations, makes that the $V \sin i$ is likely determined by the behavior of the Mg II 4481 which, as seen in Fig. 5, leads to a smaller $\delta V \sin i$ than the

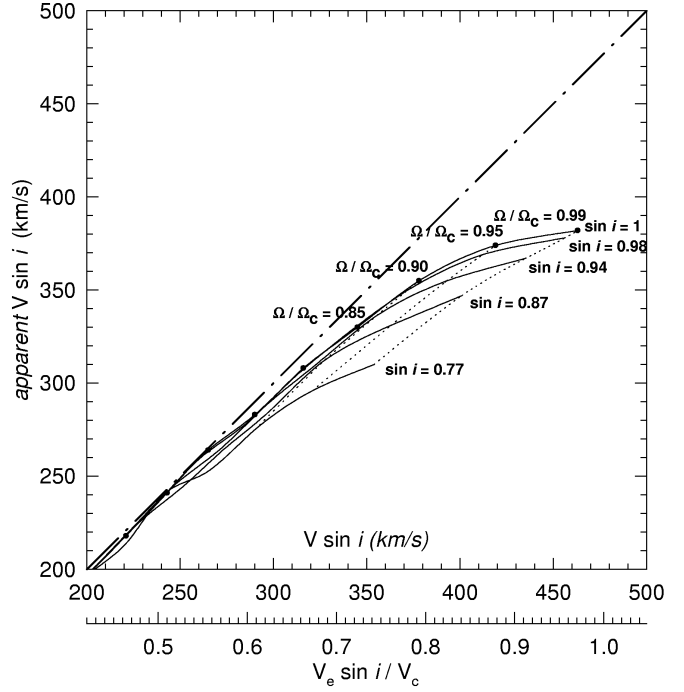


Fig. 7. Apparent and true $V \sin i$ values at $T_{\text{eff}}^o = 20000 \text{ K}$, $\log g_o = 4.0$ and different values of $\sin i$ (full-line curves) and of Ω/Ω_c (dotted curves).

He I line alone. It is then crucial that for stars with $T_{\text{eff}}^o \gtrsim 15000 \text{ K}$ both He I 4471 and Mg II 4481 are considered together in the $V \sin i$ calculation. On the contrary, for $T_{\text{eff}}^o \gtrsim 20000 \text{ K}$, the addition of $\lambda 4481 \text{ Mg II}$ in the fit does not increase significantly the accuracy of the $V \sin i$ measurements. Fig. 6 also shows that for high enough Ω/Ω_c ratios the underestimation $\delta V \sin i$ is a function of T_{eff}^o .

As the use of the $V \sin i$ parameter at a given Ω/Ω_c hides the effect of the aspect angle on the measured $V \sin i$ we plotted in Fig. 7, for a pnc B2 V spectral type, the behaviour of the apparent $V \sin i$ against its true value at different fixed inclination angles ($\sin i$). We note that the underestimation at higher $V \sin i$ is also very sensitive to the $\sin i$.

The incidence of $\log g_o$ on the underestimation $\delta V \sin i$ is further shown in Fig. 8. In this figure the relation between $\delta V \sin i$ against the true $V \sin i$ is given for different pnc effective temperatures and surface gravities. It is seen that as long as $V \sin i \lesssim 300 \text{ km s}^{-1}$, the $\delta V \sin i$ is almost independent of gravity. As soon as $V \sin i \gtrsim 300 \text{ km s}^{-1}$, not only do the $\delta V \sin i$ differences depend strongly on $\log g_o$, but depending on the effective temperature it shows two different behaviors. For temperatures $T_{\text{eff}}^o \lesssim 20000 \text{ K}$, $\delta V \sin i$ begins to decrease, while for $T_{\text{eff}}^o \gtrsim 20000 \text{ K}$ it increases even faster. In Fig. 8 the curve corresponding to $\log g_o = 3.4$ is badly determined for high $V \sin i$ values, because the gravity decreases rapidly to very low values at the equator.

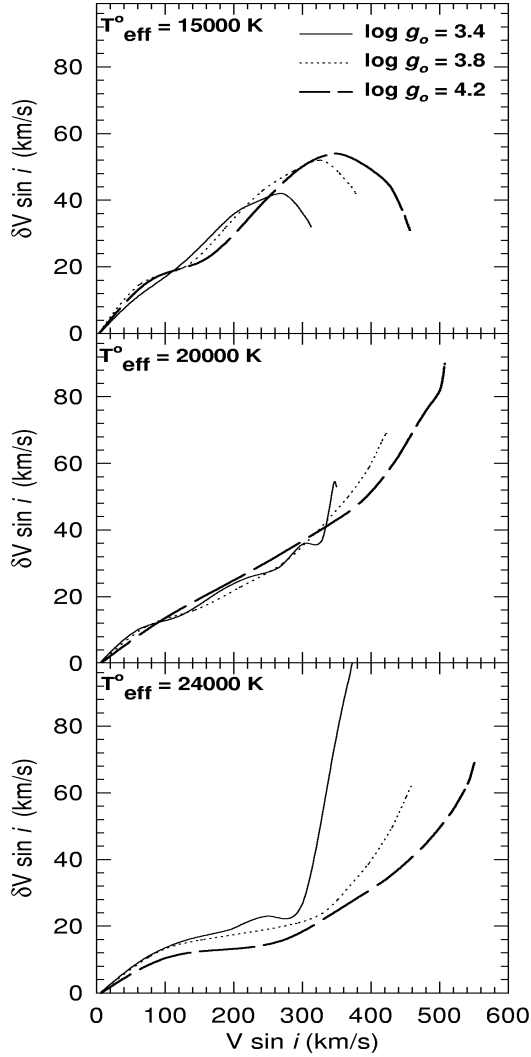


Fig. 8. $V \sin i$ lowering ($\delta V \sin i$) as a function of the true $V \sin i$ for different true effective temperature and true $\log g$ values.

5. Effects of fast rotation in other spectral regions

It is very important to know whether plane parallel model atmospheres calculated for the apparent fundamental parameters can describe accurately enough the whole observed spectrum of a rotating star. This matters not only for the study of the stellar chemical composition, but also for the energy distribution representation, which enters frequently the fundamental parameter determination. This is important, in particular, for fast rotating early type stars, whose evolution is faster than that of less massive stars, so that they are found in different evolutionary stages and can be used to test models of stellar evolution.

5.1. Chemical composition

In order to verify the reliability of the use of computed stellar spectra that ignore GD, we studied wavelength domains that contain several helium and hydrogen lines, as well as CNO spectral lines. We compared apparent spec-

tra, i.e. those computed with a plane-parallel model atmosphere using the apparent fundamental parameters given in Table 7 with pnr spectra (i.e. those calculated using FASTROT for $T_{\text{eff}}^{\text{o}}=20000$ K, $\log g_{\text{o}}=4$) and several inclination angles $\Omega/\Omega_{\text{c}}=0.99$. This comparison for hydrogen and helium lines is shown in Fig. 9. The same type of comparison for CNO elements is shown in Fig. 10. It appears then that in general REFs can be ignored for stars with $V \sin i \lesssim 150$, which correspond either to slow rotators or pole-on fast-rotators. However, in fast rotating stars seen at high inclination angles, i.e. large $V \sin i$ values, discrepancies between both series of models can be significant. Thus, the chemical composition of objects seen at high inclinations, which are also the most frequently found, must be studied using models adapted for rotating stars.

In panel (a) of Fig. 9 are shown the helium and hydrogen lines used to determine the apparent T_{eff} and $\log g$, as noted in Sect. 3.1. The spectral regions where the fit was actually performed are marked on top of spectra with horizontal thick lines. In general, these same plane-parallel models calculated and apparent fundamental parameters are representing quite satisfactorily the helium and hydrogen lines in other spectral regions (see panel (b) in Fig. 9).

The behaviour of the CNO spectral lines as function of the inclination angle and angular velocity is however more complex, as shown in Fig. 10. In Fig. 11, we reported the overabundance of oxygen and nitrogen derived for models corresponding to an *apparent* B2 IV star ($T_{\text{eff}}^{\text{app.}}=19000$ K and $\log g_{\text{app.}}=3.5$) but for different values of Ω/Ω_{c} and two different $V \sin i$ values (150 km s^{-1} and 200 km s^{-1}). The adopted fundamental parameters are listed in Table 6. This kind of modeling shows that in early B-type stars C II is expected to be underestimated when use is made of plane-parallel model atmosphere for fast rotators seen equator-on. Nevertheless, these models can still be used when stars are seen at low inclinations. The abundance of nitrogen, as derived from various N II lines, is overestimated by a plane-parallel modeling of fast rotators seen at intermediate inclination angles. In fast rotating B-type stars cooler than 25000 K, oxygen is always overestimated by plane-parallel models when fits of OII spectral lines are done, while it is expected to be somewhat underestimated if one uses the $\lambda 7772$ O I triplet.

More generally, spectral lines preferably formed at the stellar poles (N II, O II ...) tend to appear stronger when the effects of fast rotation are taken into account (see f.e. O II lines in panel (a) of Fig. 10). On the contrary, when their privileged forming region is near the equator, they often appear weaker (see f.e. O I line in panel (b) of Fig. 10) but the REFs are also generally smaller. Therefore, REFs on chemical abundance determinations strongly depend on the studied transition, on $V \sin i$ and on the effective temperature of stars. The content of CNO elements in atmospheres of early-type fast rotators, in particular Be stars, will be discussed in a forthcoming paper.

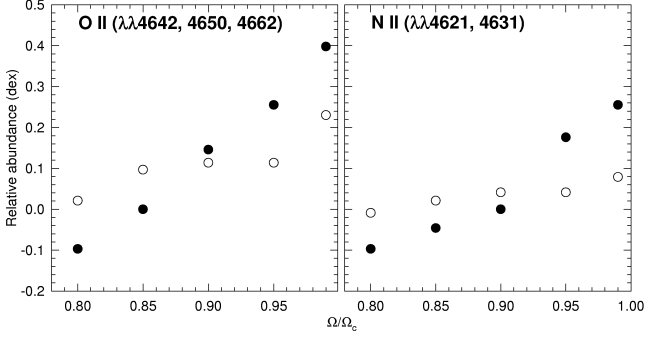


Fig. 11. Abundance overestimation in dex due to stellar flattening and gravitational darkening observed for different values of Ω/Ω_c and $V \sin i_{app}$, equal to 150 km s^{-1} (open circles) and 200 km s^{-1} (filled circles). Adopted fundamental parameters are listed in Table 6. Spectral lines used in the abundance estimate are noted in each Figure.

Table 6. Apparent (T_{eff}^{app} , $\log g_{app}$, $V \sin i_{app}$), $pnrc$ (T_{eff}^o , $\log g_o$) parameters and true $V \sin i$ used to study the effects of stellar flattening on the determination of CNO abundances (Fig. 11).

T_{eff}^{app} (K)	$\log g_{app}$	$V \sin i_{app}$ (km s^{-1})	Ω/Ω_c	T_{eff}^o (K)	$\log g_o$	$V \sin i$ (km s^{-1})	i ($^\circ$)
19000	3.5	150	0.80	19433	3.64	158	38
19000	3.5	150	0.85	19709	3.62	160	34
19000	3.5	150	0.90	19662	3.65	161	30
19000	3.5	150	0.95	19537	3.66	164	27
19000	3.5	150	0.99	20480	3.74	170	24
19000	3.5	200	0.80	19529	3.66	207	50
19000	3.5	200	0.85	19680	3.69	210	45
19000	3.5	200	0.90	20070	3.71	212	38
19000	3.5	200	0.95	20424	3.75	218	35
19000	3.5	200	0.99	20818	3.75	227	32

Table 7. True and apparent fundamental parameters used in Fig. 9 and 10 at $\Omega/\Omega_c=0.99$.

i	T_{eff}^o	$\log g_o$	$V \sin i$	T_{eff}^{app}	$\log g_{app}$	$V \sin i_{app}$
0	20000	4.0	0	18675	3.83	0
30	20000	4.0	231	18462	3.75	203
90	20000	4.0	463	16249	3.28	382

5.2. Energy distribution

Since REFs on the stellar continuum are directly proportional to the shape and apparent size of the observed stellar disk, magnitudes are very sensitive to the stellar flattening. The GD displayed by the stellar hemisphere facing the observer enhances even more these effects. REFs affect therefore the slope and the absolute level of the emitted fluxes. REFs on the stellar continuum in the visible spectral range have already been widely discussed in many previous works (Collins 1963, 1965, 1966, 1968a,b,

1974; Hardorp & Strittmatter 1968b, 1972, 1968a; Hardorp & Scholz 1971; Collins & Sonneborn 1977; Collins et al. 1991; Maeder & Peytremann 1970, 1972; Collins & Smith 1985; Zorec 1986; Pérez Hernández et al. 1999; Townsend et al. 2004). To complete the presentation of rotational effects and because the spatial UV spectral region was less explored in the literature (Kodaira & Hoekstra 1979; Llorente de Andres & Duran 1979) we show in Fig. 12 the comparison between spatial UV energy distribution computed with FASTROT using true and apparent parameters for $\Omega/\Omega_c = 0.99$ and different inclination angles. The values of parameters used in each calculation are given in Table 7. Sometimes the spatial region of stellar energy distributions are used to compare apparent diameters or to infer distances (Frémat et al. 2002). According to estimates shown in Fig. 12 differences up to 70% are expected in these quantities if they concern early type fast rotators.

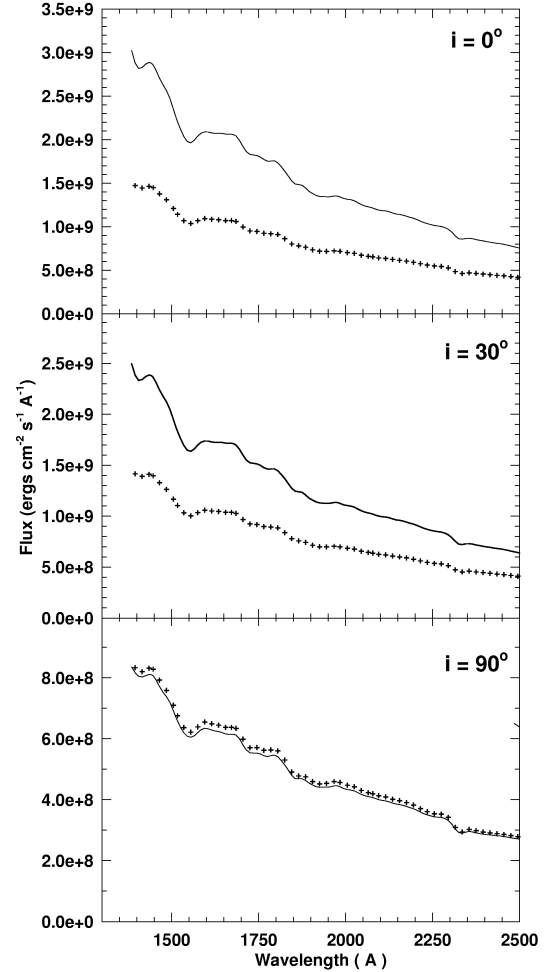


Fig. 12. Comparison between spectra computed using $pnrc$ (full line) and apparent parameters (crosses). $pnrc$ spectra were computed for $T_{eff}^o = 20000 \text{ K}$, $\log g_o = 4.0$ and $\Omega/\Omega_c = 0.99$. Three different inclination angles were considered. Apparent values for each case are given in Table 7.

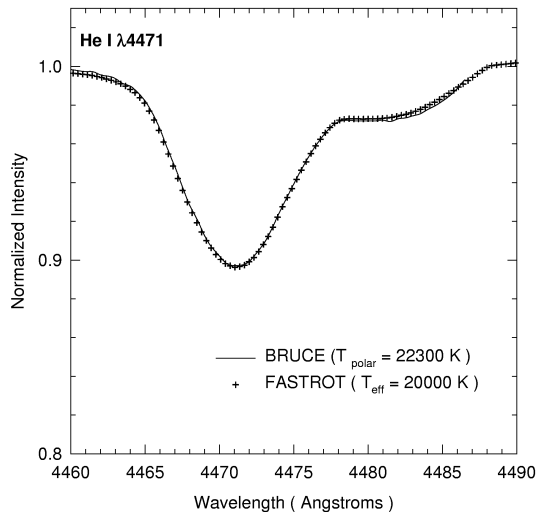


Fig. 13. Comparison between He I $\lambda 4471$ line profiles computed with BRUCE (full line, Townsend et al. 2004) and with FASTROT (crosses). Adopted input parameters in FASTROT are: $T_{\text{eff}}^{\circ} = 20000$ K, $\log g_0 = 4.0$, $\Omega/\Omega_c = 0.99$ and $V \sin i = 463$ km s $^{-1}$ (ie: polar temperature = 22300 K and polar radius = $4.03 R_{\odot}$). Adopted input parameters in BRUCE are: polar temperature = 22300 K, polar radius = $4.03 R_{\odot}$, inclination angle = 90° and equatorial velocity = 463 km s $^{-1}$.

6. Discussion

In the present approach of rotational effects on spectra emitted by early-type stars we neglected second order effects due to radiative fluxes related to the latitudinal gradient of the local effective temperature. They might be not entirely negligible (Hadrava 1992), in particular for very fast rotators, where the equatorial gravity $\lim_{\omega \rightarrow 1} g(\text{eq}) \rightarrow 0$. It is expected that their effect may reduce somewhat the GD.

6.1. Comparison with other recent calculations

To test our code, we compare in Fig. 13 the He I $\lambda 4471$ line profile computed with FASTROT and BRUCE (Townsend et al. 2004). The same model atmosphere grids were used assuming near critical rotation $\Omega/\Omega_c = 0.99$ ($V_e/V_c = 0.97$) and inclination $i = 90^{\circ}$. Relations (5) and (6) were combined to find what pnr effective temperature is implied by the T_{polar} value we used as entry parameter in BRUCE. This procedure leads to an almost identical gravitational darkening and to identical line profiles as shown in Fig. 13. We made several comparisons of FASTROT and BRUCE results of the type shown in Fig. 13. Although our integration algorithms is different and outnumbers the equivalent elementary surface elements those of BRUCE, quite similar results are obtained. The only difference between both approaches relies on the adopted fundamental parameters. In FASTROT a unique set of pnr T_{eff}° and mass M is used for the whole series of Ω values, while BRUCE does allow to specify the temperature distri-

bution in 2 possible ways: by fixing T_{polar} or by fixing the bolometric luminosity (see eq. 3 in Townsend et al. 2004).

6.2. Implications for the study of Be stars

It has been pointed out by Stoeckley (1968) and Townsend et al. (2004) that the FWHM of the $\lambda 4471$ He I line can converge to a constant value at high $V \sin i$ when the stellar angular velocity approaches the critical rotation, which makes that the $V \sin i$ values of fast rotators, in particular those of Be stars, can be underestimated. Nevertheless, the implication on the measurements of $V \sin i$ in actual early-type stars by taking into account entirely the blend He I $\lambda 4470 + \text{He I } \lambda 4471 + \text{Mg II } \lambda 4481$, has still not been entirely explored. Our comparisons between true and apparent values obtained using the fitting procedure (CASE A Table 3), which mimic real cases of $V \sin i$ determination, show that there is a progressive lowering of the $V \sin i$ for increasing rotational rates. We also see that this $V \sin i$ underestimation does not imply necessarily a saturation of the estimated projected rotation velocity, even there is critical rotation (see Fig. 6).

It is interesting then to revisit the most probable value of the Ω/Ω_c rate of Be stars if the REFs are taken into account. Chauville et al. (2001) have studied a sample of 116 Be stars and determined their $V \sin i_{\text{app}}$ parameter without taking into account the REFs. They used, however, Stoeckley and Mihalas' (1973) calculations of rotationally broadened lines, where the wavelength dependent limb-darkening within the line profiles is considered and which ensures that there is no systematic underestimation of rotational parameters, effect that was discussed by Collins & Truax (1995). Chauville et al. (2001) have thus concluded that on average Be stars rotate at $\Omega/\Omega_c \sim 0.8$. We have studied these stars again, and some others, and redetermined carefully their *apparent* fundamental parameters by fitting their spectra with model atmospheres without rotation. We adopted the *apparent* $V \sin i$ determined by Chauville et al. (2001) in order to avoid underestimations of these quantity produced by the Fourier method, which uses a constant limb-darkening coefficient in the frequencies over the line profile. Using our GRIDB of synthetic spectra, we have determined the pnr fundamental parameters of the program objects, in particular their $V \sin i$. These parameters were calculated for an average Ω/Ω_c rate, the same for all stars and whose value was iterated. The iteration started first by assuming $\Omega/\Omega_c = 0.8$. At each iteration step we corrected the *apparent* fundamental parameters in order to obtain the pnr ones and redetermined, hence, the ratios $V \sin i/V_c$ of each stars and studied its distribution. Each time we derived from the distribution the average of Ω/Ω_c and its mode, i.e. the most frequent or probable value of Ω/Ω_c . These quantities were estimated in two ways: a) using the same method as Chauville et al. (2001); b) determining the average and the mode of V/V_c by correcting the distribution of $V \sin i/V_c$ for the $\sin i$ effect. Since the mode of a given

distribution depends on at least its first four moments, where errors increase with the order of the moment, we iterated the average Ω/Ω_c . We also started the iteration assuming all stars rotate at $\Omega/\Omega_c = 1.0$. We note that each apparent effective temperature, gravity and projected rotational velocity was considered with its 2σ error. The interval $(X - 2\sigma_X, X + 2\sigma_X)$ corresponding to each *apparent* X parameter was divided into eight parts, so that we had 9 entries for each independent parameter. This produced 9^3 determinations of each corresponding pncr X parameter or true $V\sin i$. Since each distribution of the obtained pncr parameters is not symmetrical, we adopted its mode to represent the corresponding most probable solution of the sought pncr parameter.

Both iterations ended at the same values of the average Ω/Ω_c and the mode:

$$\overline{\Omega/\Omega_c} = 0.85_{-0.04}^{+0.06} \quad (\Omega/\Omega_c)_{mode} = 0.88_{-0.04}^{+0.06} \quad (8)$$

Table 8 summarizes the characteristics of iterations. Moments μ_n are for V/V_c distributions. The program stars and their fundamental parameters are given in Table 9. In this table are given the apparent effective temperature, surface gravity and rotational parameter with their respective 1σ errors. The modes of the corresponding pncr parameter and of the corrected $V\sin i$ are also listed, as well as the critical equatorial velocity, the estimated inclination angle and the 1σ dispersion of the respective 9^3 determinations of each fundamental parameter.

From the rates displayed in (8) we see that critical rotation among Be stars is reachable only by a fraction of objects between 2 and 3σ interval beyond the $(\Omega/\Omega_c)_{mode}$. While the difference between *apparent* and *true* $V\sin i$ values seems to be significant in some cases, the increase of Ω/Ω_c is not so high, as compared to the ratio obtained by Chauville et al. (2001) with *apparent* $V\sin i$ parameters. This is simply due to the fact that we need to consider also the increase from *apparent* to pncr values of the stellar fundamental parameters. These last identify objects that are more massive and less evolved than expected from the *apparent* parameters. Such increase also implies a significant augmentation of the equatorial critical velocity V_c which is barely overweighted by the respective *true* $V\sin i$ value.

Table 8. Iteration of $\overline{\Omega/\Omega_c}$ and $(\Omega/\Omega_c)_{mode}$

Ω/Ω_c	$\overline{V/V_c}$	$\overline{\Omega/\Omega_c}$	modes				
			V/V_c	Ω/Ω_c	μ_2	μ_3	μ_4
0.800	0.708	0.842	0.756	0.879	0.507	0.369	0.271
0.842	0.712	0.846	0.753	0.878	0.513	0.375	0.277
0.846	0.713	0.847	0.746	0.872	0.515	0.376	0.277
0.847	0.713	0.847	0.751	0.876	0.515	0.376	0.278
1.000	0.782	0.898	0.726	0.854	0.627	0.513	0.428
0.898	0.725	0.856	0.673	0.814	0.533	0.397	0.300
0.856	0.715	0.848	0.733	0.862	0.518	0.379	0.281
0.848	0.713	0.846	0.732	0.861	0.514	0.376	0.278
0.846	0.713	0.847	0.751	0.876	0.514	0.375	0.277

6.2.1. Comments on the solutions obtained

We remind that the values of parameters displayed in Table 9 are 'modes' of the respective distributions of 9^3 possible solutions. They can be considered as representing the most probable configuration of fundamental parameters for the rotating star, as they are perceived from the entry set of *apparent* parameters with their uncertainties, seen through the models calculated with FASTROT used to interpret them. They look like a sort of independent "determinations" which also seem sometimes to underestimate the effects due to fast rotation. Nevertheless, if we used only the *apparent* entry parameters without their uncertainties, the unique translation into pncr quantities that comes out would lead in many cases to ΔT_{eff} , $\Delta \log g$ and $\Delta V\sin i$ differences between pncr and *apparent* values that are higher than those issued from the values in Table 9. We calculated the $\overline{\Omega/\Omega_c}$ and $(\Omega/\Omega_c)_{mode}$ using these simplified estimates of pncr parameters and true $V\sin i$, as well as the same iteration procedure for Ω/Ω_c . We obtained thus, $\overline{\Omega/\Omega_c} = 0.83$, near the value put forward in Zorec et al. (2003) and $(\Omega/\Omega_c)_{mode} = 0.88$. This small increase of the Ω/Ω_c , as compared to the value obtained by Chauville et al. (2001), is entirely ascribed to the higher V_c values implied by the *apparent* \rightarrow pncr transformation of fundamental parameters.

6.2.2. pncr and actual fundamental parameters

In this paper, we have studied the relation between the *apparent* parameters and those that should represent the actual stellar mass and its evolutionary stage. The translation obtained into pncr parameters was performed with the help of evolutionary tracks calculated for non rotating stars (Schaller et al. 1992). However, evolutionary tracks of rotating objects are somewhat different (Heger & Langer 2000; Meynet & Maeder 2000). Depending on the case, they may produce slightly different mass estimates. These estimates are those which we might finally consider as a better approach to the *actual* stellar mass. Nevertheless, the mentioned differences are altogether small and do not modify whatsoever the results obtained in the preceding sections. Their *ins* and *outs* are out of the scope of the present work and will be widely discussed in another contribution.

7. Conclusions

In this paper we present the calculation code FASTROT to calculate the effects carried by fast rotation on the fundamental parameters of early-type stars. Particular attention is paid to represent hydrogen Balmer, He I and Mg II lines in the blue spectral region, which are currently used to infer from spectroscopic data the fundamental parameters of early-type stars. We also calculated a number of C, N and O lines in the visible spectral range, which enter the CNO abundance determination.

We have calculated synthetic spectra with classical plane-parallel non-LTE model atmospheres using *apparent* fundamental parameters derived from $H\gamma$, $He\text{I}4471$ and $Mg\text{II}4481$ lines and compared their predictions for other spectral regions of rotating stars. We noted that the above *apparent* fundamental reliably reproduce also the remaining Balmer and $He\text{I}$ lines in the visual. However, discrepant fits are expected for CNO lines. The noted discrepancies may thus lead to systematic overestimates of the N abundances, while the C abundances can be underestimated. Regarding the O abundance, it depends on the lines used. They are sensitive to local formation conditions and reflect preferences either on the polar or equatorial formation regions. O abundances can then be under- or overestimated, depending on the lines used, stellar apparent configuration, if rotational effects are neglected.

The fastest rotation in the main sequence are probably Be stars. The strong gravitational darkening can lead then to sensitive $V\sin i$ underestimations, which in turn may imply that the hitherto undercritical rotation of these stars can be argued. We payed much attention then on the determination of the fundamental parameters of fast rotators, in particular on $V\sin i$. We thus obtained that although the classical $V\sin i$ parameter do underestimate the stellar equatorial velocity of fast rotators, the fact that the pncr stellar mass is higher and the evolutionary stage lower than expected from *apparent* quantities, causes that in most cases the increase in the estimate of $V\sin i$ does not overweights considerably the new V_c . The study of a sample of 130 Be stars leads thus to a most probable ratio $V_e/V_c \simeq 0.75$, or $\Omega/\Omega_c \simeq 0.88$, which still imply average undercritical surface rotation.

Acknowledgements. We are grateful to the referee Dr. I.D. Howarth and to Dr. R. Townsend for their comments and suggestions helped to improve the presentation of our results. YF thanks Dr. P.Lampens for hosting him at the Royal Observatory of Belgium and acknowledges funding from the Belgian 'Diensten van de Eerste Minister - Federale Diensten voor Wetenschappelijke, Technische en Culturele Aangelegenheden' (Research project MO/33/007).

References

- Barnard, A. J., Cooper, J., & Shamey, L. J. 1969, *A&A*, 1, 28
- Bodenheimer, P. 1971, *ApJ*, 167, 153
- Chauville, J., Zorec, J., Ballereau, D., et al. 2001, *A&A*, 378, 861
- Claret, A. 1998, *A&A*, 335, 647
- Claret, A. 2000, *A&A*, 359, 289
- Clement, M. J. 1979, *ApJ*, 230, 230
- Collins, G. W. 1963, *ApJ*, 138, 1134
- Collins, G. W. 1965, *ApJ*, 142, 265
- Collins, G. W. 1966, *ApJ*, 146, 914
- Collins, G. W. 1968a, *ApJ*, 151, 217
- Collins, G. W. 1968b, *ApJ*, 152, 847
- Collins, G. W. 1974, *ApJ*, 191, 157
- Collins, G. W. & Smith, R. C. 1985, *MNRAS*, 213, 519
- Collins, G. W. & Sonneborn, G. H. 1977, *ApJS*, 34, 41
- Collins, G. W. & Truax, R. J. 1995, *ApJ*, 439, 860
- Collins, G. W., Truax, R. J., & Cranmer, S. R. 1991, *ApJS*, 77, 541
- Cunto, W., Mendoza, C., Ochsenbein, F., & Zeippen, C. J. 1993, *A&A*, 275, L5
- Didelon, P. 1982, *A&AS*, 50, 199
- Endal, A. S. & Sofia, S. 1976, *ApJ*, 210, 184
- Endal, A. S. & Sofia, S. 1979, *ApJ*, 232, 531
- Frémat, Y., Zorec, J., Hubert, A.-M., et al. 2002, *A&A*, 385, 986
- Gray, R. O. & Corbally, C. J. 1994, *AJ*, 107, 742
- Hadrava, P. 1992, *A&A*, 256, 519
- Hardorp, J. & Scholz, M. 1971, *A&A*, 13, 353
- Hardorp, J. & Strittmatter, P. A. 1968a, *ApJ*, 153, 465
- Hardorp, J. & Strittmatter, P. A. 1968b, *ApJ*, 151, 1057
- Hardorp, J. & Strittmatter, P. A. 1972, *A&A*, 17, 161
- Heger, A. & Langer, N. 2000, *ApJ*, 544, 1016
- Hubeny, I. & Lanz, T. 1995, *ApJ*, 439, 875
- Kodaira, K. & Hoekstra, R. 1979, *A&A*, 78, 292
- Kurucz, R. L. 1993, Kurucz CD-ROM No.13. Cambridge, Mass.: Smithsonian Astrophysical Observatory.
- Lanz, T. & Hubeny, I. 2003, *ApJS*, 146, 417
- Leckrone, D. S. 1971, *A&A*, 11, 387
- Llorente de Andres, F. & Duran, C. M. 1979, *A&A*, 72, 318
- Lucy, L. B. 1967, *Zeitschrift fur Astrophysics*, 65, 89
- Maeder, A. & Meynet, G. 1996, *A&A*, 313, 140
- Maeder, A. & Meynet, G. 2000, *A&A*, 361, 159
- Maeder, A. & Peytremann, E. 1970, *A&A*, 7, 120
- Maeder, A. & Peytremann, E. 1972, *A&A*, 21, 279
- Meynet, G. & Maeder, A. 2000, *A&A*, 361, 101
- Mihalas, D., Barnard, A. J., Cooper, J., & Smith, E. W. 1974, *ApJ*, 190, 315
- Moss, D. & Smith, R. C. 1982, *Reports of Progress in Physics*, 44, 831
- Pérez Hernández, F., Claret, A., Hernández, M. M., & Michel, E. 1999, *A&A*, 346, 586
- Pinsonneault, M. H., Deliyannis, C. P., & Demarque, P. 1991, *ApJ*, 367, 239
- Reiners, A. 2003, *A&A*, 408, 707
- Sackmann, I. J. 1970, *A&A*, 8, 76
- Schaller, G., Schaerer, D., Meynet, G., & Maeder, A. 1992, *A&AS*, 96, 269
- Sigut, T. A. A. 1996, *ApJ*, 473, 452
- Slettebak, A., Collins, G. W., Parkinson, T. D., Boyce, P. B., & White, N. M. 1975, *ApJS*, 29, 137
- Smith, C. R. & Worley, R. 1974, *MNRAS*, 167, 199
- Stoeckley, T. R. 1968, *MNRAS*, 140, 149
- Tassoul, J. 1978, *Theory of rotating stars* (Princeton Series in Astrophysics, Princeton: University Press, 1978)
- Townsend, R. H. D., Owocki, S. P., & Howarth, I. D. 2004, *MNRAS*, 350, 189
- Tuominen, J. 1972, *Astrophys. Lett.*, 10, 175
- Varosi, F., Lanz, T., deKoter, A., et al. 1995, <ftp://idlastro.gsfc.nasa.gov/pub/contrib/varosi/modion>
- Vidal, C. R., Cooper, J., & Smith, E. W. 1973, *ApJS*, 25,

37

Zahn, J.-P. 1992, *A&A*, 265, 115

Zeipel, H. V. 1924, *MNRAS*, 84, 665

Zorec, J. 1986, PhD Thesis: Structure et rotation différentielle dans les étoiles B avec et sans émission (Paris: Université VII, 1986)

Zorec, J., Frémat, Y., Ballereau, D., et al. 2003, in SF2A-2003: Semaine de l'Astrophysique Française, 617

Zorec, J., Mochkovitch, R., & Divan, L. 1988, *Académie des Sciences Paris Comptes Rendus Serie Sciences Mathématiques*, 306, 1265

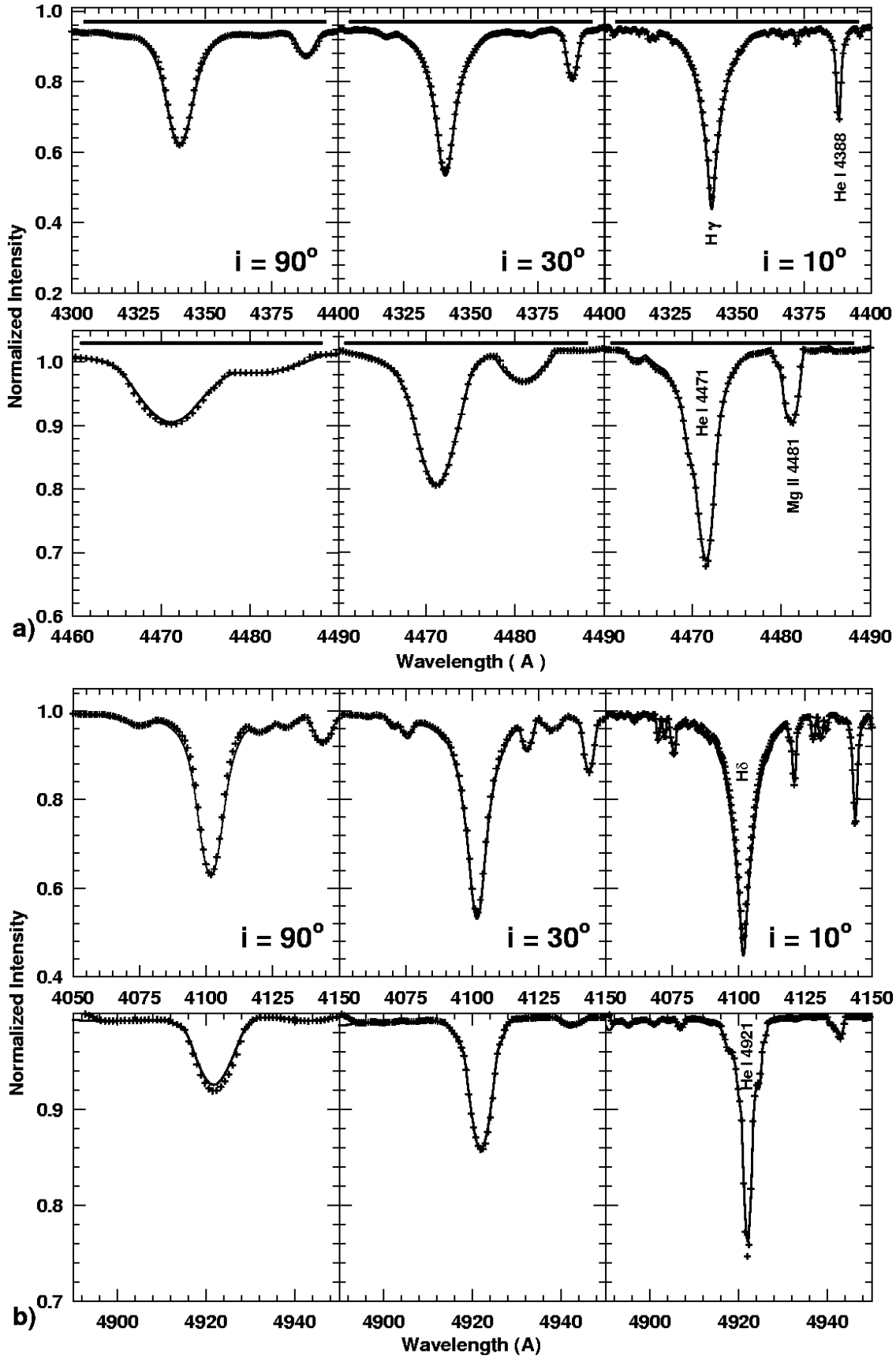


Fig. 9. Comparison between spectra computed using pncr (full line) and apparent parameters (crosses). Pncr spectra were computed for $T_{\text{eff}}^{\circ} = 20000$ K, $\log g_o = 4.0$ and $\Omega/\Omega_c = 0.99$. Three different inclination angles were considered. The values of the apparent parameters for each case are given in Table 7.

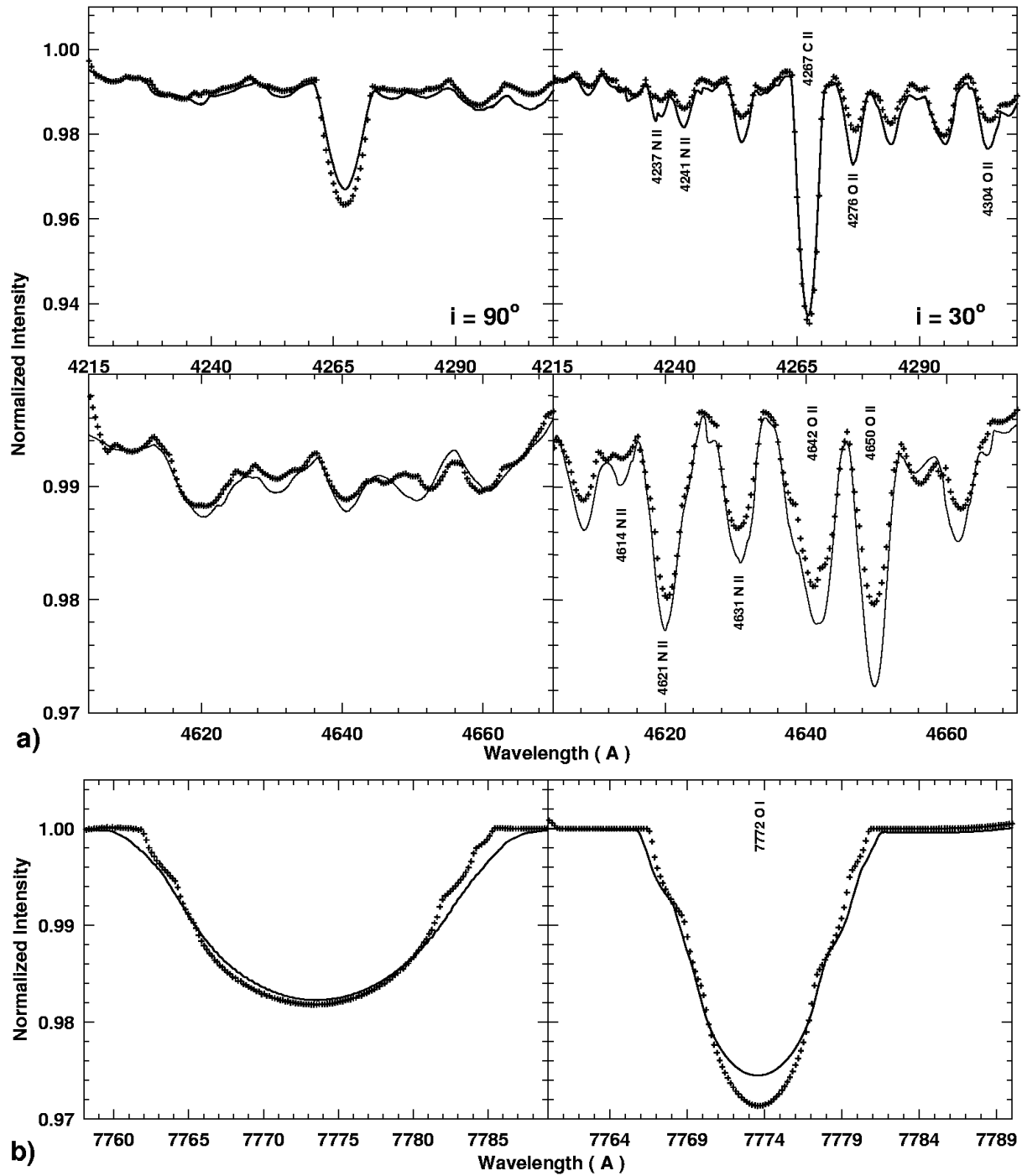


Fig. 10. Comparison between spectra computed using pnrc (full line) and apparent parameters (crosses). Pnrc spectra were computed for $T_{\text{eff}}^{\circ} = 20000$ K, $\log g_0 = 4.0$ and $\Omega/\Omega_c = 0.99$. Three different inclination angles were considered. Apparent values for each case are given in Table 7.

Table 9: Apparent and pncrc fundamental parameters of the studied stars. An electronic version of the table will be made available at the CDS.

HD	<i>Apparent parameters</i>			<i>Mode of the pncrc parameters</i>				
	$T_{\text{eff}} \pm \epsilon$	$\log g \pm \epsilon$	$V \sin i \pm \epsilon$	$T_{\text{eff}} \pm 1\sigma$	$\log g \pm 1\sigma$	$V \sin i \pm 1\sigma$	$V_c \pm 1\sigma$	$i^\circ \pm 1\sigma$
144	11956±324	3.383±0.055	125±07	12206±414	3.403±0.067	132±08	309±20	33.9±1.2
4180	14438±272	3.284±0.041	195±10	15584±426	3.399±0.062	208±13	332±21	55.7±3.2
5394	26431±618	3.800±0.070	432±28	30001±624	3.990±0.065	441±27	577±36	76.4±2.7
6811	12478±444	3.092±0.068	85±05	12578±481	3.110±0.073	93±06	274±19	26.5±1.0
10516	25556±659	3.899±0.078	440±30	29031±751	4.168±0.087	462±33	590±42	72.5±3.9
11606	19484±297	3.653±0.037	280±14	21422±439	3.774±0.055	286±16	446±26	58.2±3.5
18552	12715±284	3.456±0.048	286±16	14646±244	3.776±0.041	292±14	369±19	75.2±5.0
19243	21243±388	3.270±0.043	160±08	22752±409	3.297±0.043	165±09	387±21	36.2±1.3
20336	18684±517	3.865±0.072	328±21	20843±558	4.050±0.076	341±23	487±32	66.7±4.0
22192	15767±509	3.465±0.074	275±19	17690±299	3.763±0.042	295±15	397±20	75.0±3.1
22780	13299±284	3.381±0.046	285±15	15686±443	3.572±0.066	297±18	366±23	90.0±1.0
23016	12230±241	3.922±0.047	235±12	13420±249	4.012±0.047	242±12	410±21	48.7±2.6
23302	12754±504	3.368±0.078	170±12	13484±293	3.412±0.047	181±10	320±18	46.8±1.6
23480	13691±481	3.629±0.076	240±16	14828±402	3.792±0.064	254±15	391±24	57.3±3.3
23552	12711±416	3.764±0.070	220±14	13708±239	3.807±0.043	230±12	387±20	52.0±2.2
23630	12258±505	3.047±0.076	140±10	12885±292	3.095±0.045	149±08	274±15	44.6±1.6
23862	12106±272	3.937±0.052	286±16	13436±257	4.197±0.050	290±15	420±22	65.3±3.9
24534	25191±513	3.618±0.056	293±17	26831±699	3.854±0.081	294±20	480±34	54.7±2.6
25940	16158±582	3.572±0.084	197±14	17593±338	3.789±0.049	220±13	386±21	38.3±4.5
28497	26724±427	4.200±0.046	335±17	28101±738	4.222±0.088	342±24	631±45	45.4±2.0
30076	20488±330	3.772±0.041	213±11	21311±397	3.792±0.049	225±12	456±25	38.4±1.7
32343	16131±514	3.798±0.077	95±06	16121±430	3.790±0.065	103±06	410±26	19.7±0.8
33328	21137±599	3.447±0.075	318±22	24340±644	3.608±0.076	333±23	440±30	73.0±2.4
35411	23652±510	3.711±0.059	170±10	25138±441	3.719±0.046	174±09	484±26	29.0±1.3
35439	22134±665	3.920±0.087	263±19	23547±364	3.948±0.041	266±13	513±26	42.2±2.3
36576	22618±508	3.804±0.062	265±16	24502±399	3.839±0.043	266±13	487±25	46.3±2.2
37202	19310±550	3.732±0.075	310±7	21460±420	3.910±0.060	326±7	466±13	66.0±4.1
37657	17951±542	3.659±0.076	198±13	19275±301	3.686±0.039	209±10	427±21	41.9±1.9
37795	12963±203	3.517±0.036	180±09	13695±437	3.559±0.069	192±12	355±23	44.9±2.1
37967	16543±264	3.850±0.041	210±10	17558±589	3.873±0.085	228±16	455±33	42.1±2.1
38010	25826±448	4.089±0.050	370±20	28015±555	4.194±0.061	377±22	608±36	53.0±3.4
40978	18227±571	3.576±0.078	200±14	19605±550	3.608±0.073	211±14	401±27	43.3±1.9
41335	20902±610	3.886±0.081	358±25	23431±639	4.076±0.082	376±26	520±36	68.5±3.8
42545	15764±334	3.849±0.053	285±16	17522±309	3.976±0.046	303±16	460±24	60.1±4.0
44458	22914±532	3.600±0.063	242±15	24745±667	3.640±0.079	254±18	449±31	48.0±2.1
45314	29160±467	3.949±0.044	285±14	31092±557	3.968±0.053	291±16	594±33	40.6±1.9
45542	13711±526	3.627±0.082	217±15	14651±229	3.682±0.038	226±11	369±18	52.5±2.6
45725	17810±455	3.895±0.066	330±20	19601±459	4.168±0.065	345±21	486±30	66.6±3.9
45910	20659±484	2.739±0.052	240±14	22983±471	2.992±0.048	254±14	342±20	76.5±3.5
45995	21198±632	3.769±0.083	255±18	22674±423	3.806±0.050	260±14	470±26	46.8±2.1
47054	12336±481	3.538±0.078	219±15	13292±355	3.607±0.058	227±13	351±21	57.2±2.2
48917	20341±435	3.395±0.053	205±12	21348±569	3.438±0.070	212±14	389±26	45.4±2.0
50013	24627±590	4.017±0.072	243±15	25790±713	4.026±0.087	244±17	535±39	37.3±1.9
50083	20908±604	3.678±0.078	170±12	21216±625	3.689±0.081	176±12	452±32	32.5±1.4
53974	27808±759	3.650±0.085	100±17	27624±577	3.649±0.060	107±06	490±30	16.5±0.6
54309	20859±397	3.587±0.048	195±10	22235±543	3.610±0.066	201±13	425±27	38.4±1.5
56014	18544±614	3.287±0.081	280±20	21061±453	3.514±0.055	290±17	389±23	72.6±4.2
56139	19537±331	3.615±0.042	85±04	19465±300	3.612±0.037	89±04	403±20	16.6±0.7
57219	19865±575	3.874±0.078	80±05	19759±486	3.862±0.066	84±05	443±28	14.3±0.7
58050	19961±465	3.934±0.063	130±08	19998±590	3.926±0.081	136±09	481±34	21.9±1.2
58343	16531±409	3.619±0.059	43±02	16389±437	3.611±0.063	49±03	377±24	9.7±0.3
58715	11772±344	3.811±0.062	230±14	12769±395	3.858±0.068	231±14	380±24	54.5±2.9

58978	24445±476	4.153±0.057	370±21	26622±717	4.203±0.088	375±26	615±44	55.2±3.0
60606	18030±332	3.662±0.045	273±14	19600±414	3.783±0.055	285±16	441±25	58.2±3.6
60848	27685±671	4.051±0.077	247±16	28491±630	4.057±0.070	256±16	582±37	35.4±1.8
63462	26558±635	3.598±0.070	440±29	30685±728	3.835±0.077	514±31	545±37	90.0±1.0
65875	20205±532	3.845±0.071	153±10	20358±590	3.844±0.079	163±11	447±31	27.8±1.2
68980	25126±642	3.951±0.077	145±09	25172±492	3.945±0.056	152±08	534±31	22.2±1.2
75311	16943±429	3.846±0.064	268±16	18513±527	4.089±0.077	283±19	467±31	54.2±4.0
77320	19555±488	3.871±0.067	345±22	21539±637	4.015±0.085	349±25	501±36	68.7±3.6
83953	15187±329	3.661±0.051	260±14	16616±273	3.788±0.041	276±14	407±21	61.0±4.0
86612	16374±577	3.580±0.083	185±13	17392±381	3.790±0.055	206±12	381±22	43.3±4.2
88661	21527±384	3.989±0.049	237±12	22334±450	4.003±0.057	243±14	511±29	39.0±2.1
89080	11720±431	3.339±0.070	240±16	13275±251	3.581±0.043	245±13	320±17	70.8±3.0
91120	11120±428	3.881±0.076	295±21	12592±244	4.171±0.050	310±16	407±21	70.7±2.7
91465	17389±415	3.518±0.057	266±16	19338±582	3.704±0.079	285±20	401±28	67.3±3.7
105435	22360±589	3.916±0.075	260±17	23384±446	3.942±0.053	263±14	527±29	41.6±2.3
105521	16371±451	3.097±0.060	120±07	17490±409	3.124±0.052	128±07	320±19	33.4±1.1
109387	13982±392	3.479±0.061	200±12	15383±357	3.582±0.054	209±12	362±21	50.0±2.6
110432	20324±344	3.638±0.042	400±21	24070±603	3.950±0.074	419±28	485±32	85.4±0.3
112078	16484±409	4.028±0.063	302±18	18398±331	4.281±0.051	327±17	506±27	56.3±3.6
112091	20349±541	3.934±0.073	210±14	21649±638	3.944±0.084	221±15	492±35	36.0±1.9
120324	22554±661	3.906±0.085	159±11	22698±533	3.904±0.067	166±10	508±32	25.7±1.3
120991	22214±631	3.685±0.079	70±04	22063±414	3.679±0.049	75±04	429±23	13.0±0.5
124367	17508±429	3.757±0.061	295±18	19720±310	3.914±0.041	318±16	446±22	62.9±5.1
127972	19798±525	3.846±0.071	310±20	21761±565	3.969±0.074	326±21	500±33	57.8±3.8
131492	18353±576	3.535±0.078	185±13	19660±392	3.564±0.050	195±11	395±22	41.0±1.9
135734	12705±240	3.737±0.044	278±14	14483±383	4.005±0.064	282±17	391±24	68.7±4.0
137387	22920±456	4.162±0.058	250±14	23719±550	4.167±0.069	251±16	573±36	34.6±1.8
138749	14457±401	3.745±0.064	340±21	16808±566	3.932±0.084	345±24	441±31	79.7±3.8
142184	21246±397	4.200±0.053	340±18	22649±640	4.238±0.085	342±24	574±41	51.5±2.4
142926	12076±403	3.917±0.071	336±22	13866±339	4.188±0.061	338±20	424±25	73.8±2.0
142983	17645±554	3.845±0.080	390±27	20104±389	4.041±0.053	407±22	501±28	67.4±3.7
148184	28783±727	3.913±0.081	144±10	28762±611	3.908±0.065	151±09	580±36	20.0±0.9
149438	28959±526	3.739±0.051	15±03	28590±610	3.732±0.063	15±03	536±33	2.3±0.1
149757	26378±729	3.795±0.086	340±25	28797±638	4.047±0.070	352±22	534±34	60.7±3.3
157042	21787±533	4.062±0.070	340±22	23711±639	4.310±0.084	348±24	572±40	53.1±3.7
158427	18044±310	3.991±0.046	290±15	19586±327	4.232±0.047	305±15	477±24	51.3±3.2
162732	13523±243	3.754±0.043	310±16	15448±560	3.975±0.087	321±23	431±31	72.9±2.6
164284	21609±523	3.943±0.068	280±17	22822±670	3.978±0.087	287±21	513±37	48.0±2.4
167128	17396±608	3.645±0.086	48±03	17254±575	3.637±0.082	55±03	389±28	10.6±0.3
173948	22075±472	3.599±0.056	140±08	22212±517	3.606±0.062	150±09	430±27	27.3±1.1
174237	17683±556	3.764±0.079	163±11	18458±441	3.773±0.061	173±10	425±26	33.2±1.5
175869	12241±496	3.254±0.077	175±12	13442±441	3.474±0.069	182±12	311±20	52.0±2.1
178175	18939±286	3.489±0.035	105±05	18976±561	3.493±0.074	111±07	396±27	22.4±1.1
183656	12626±524	3.295±0.081	270±20	14642±360	3.551±0.056	284±16	354±21	76.7±4.9
183914	13218±445	3.830±0.074	220±14	14422±278	3.867±0.048	228±12	387±21	48.7±2.3
184915	27076±540	3.492±0.054	229±13	28888±606	3.528±0.060	244±15	479±29	41.1±2.5
185037	12058±212	3.768±0.042	280±14	13586±523	4.002±0.086	287±20	410±29	68.4±3.6
187811	18086±583	3.810±0.083	245±17	19682±336	3.849±0.044	258±13	434±22	48.9±2.4
189687	18106±379	3.455±0.050	200±11	19336±319	3.498±0.039	212±11	395±20	46.6±2.3
191610	18353±516	3.718±0.072	300±20	20671±587	3.983±0.079	318±22	442±30	63.7±3.9
192044	12570±490	3.366±0.077	245±17	14452±221	3.573±0.036	248±12	332±16	71.1±3.1
193911	12467±424	3.090±0.065	160±10	13434±352	3.194±0.053	168±10	292±17	49.1±2.0
194335	22120±373	4.071±0.047	360±19	24357±458	4.185±0.055	363±20	581±32	57.6±3.9
198183	13925±332	3.167±0.049	125±07	14233±404	3.195±0.059	133±08	300±19	35.6±1.5
200120	21750±655	3.784±0.085	379±27	24808±520	3.966±0.061	387±23	530±32	73.2±3.2
201733	16350±504	3.943±0.077	340±23	18410±375	4.176±0.056	357±20	481±27	68.4±4.8
203374	24645±660	3.458±0.076	333±23	27662±651	3.663±0.070	342±22	477±31	70.7±3.7
203467	17087±521	3.377±0.072	153±10	18249±575	3.404±0.077	165±11	356±25	38.2±1.4

205637	17801±470	3.442±0.063	225±14	19348±351	3.673±0.045	238±12	395±21	54.7±2.7
206773	29154±746	3.885±0.083	390±28	31800±547	4.143±0.052	399±21	617±33	62.1±3.6
208057	17974±396	3.675±0.055	100±05	17977±510	3.672±0.071	110±07	391±26	20.6±0.9
208682	22114±652	3.977±0.086	307±22	23814±617	4.019±0.077	314±21	525±36	53.3±2.9
209014	12016±408	3.155±0.064	320±21	14694±509	3.571±0.077	357±21	343±24	90.0±1.0
209409	12942±402	3.701±0.067	280±18	14562±514	3.978±0.082	282±20	391±27	69.9±3.4
209522	16581±408	3.704±0.060	275±16	18507±279	3.886±0.039	299±14	430±21	66.6±4.3
210129	13515±240	3.421±0.040	130±06	14127±444	3.439±0.068	140±09	326±21	33.8±1.4
212076	19270±326	3.726±0.043	98±05	19236±419	3.721±0.056	103±06	439±26	18.6±0.9
212571	26061±736	3.915±0.088	230±17	27574±645	3.926±0.072	233±15	558±37	33.6±1.7
214168	25827±434	4.200±0.049	300±16	27647±688	4.211±0.081	305±21	619±43	40.0±1.7
214748	11966±356	3.375±0.059	200±12	13294±437	3.606±0.070	205±13	317±21	56.9±2.6
217050	17893±509	3.571±0.070	340±22	20723±612	3.871±0.082	355±25	443±31	78.5±2.1
217543	17237±584	3.685±0.083	325±24	19569±366	3.933±0.050	335±18	440±24	74.9±3.9
217675	14052±439	3.229±0.065	274±19	16741±469	3.460±0.066	289±17	343±22	90.0±1.0
217891	14359±295	3.672±0.048	95±05	14376±449	3.668±0.070	100±06	367±24	20.7±1.0
224544	14799±279	3.364±0.042	260±14	16557±460	3.560±0.066	270±17	373±24	72.8±2.6
224559	15914±329	3.597±0.049	300±16	18338±412	3.809±0.058	312±18	427±25	75.8±3.7
224686	11286±218	3.671±0.044	290±16	12800±281	3.948±0.052	300±16	380±21	76.1±2.7